

1 **Variation of sediment supply by periglacial debris flows at Zelunglung**  
2 **in the eastern syntaxis of Himalayas since the 1950 Assam Earthquake**

3 Kaiheng Hu<sup>1,2</sup>, Hao Li<sup>1,2,3</sup>, Shuang Liu<sup>1,2</sup>, Li Wei<sup>1,2</sup>, Xiaopeng Zhang<sup>1,2,3</sup>, Limin Zhang<sup>4</sup>, Bo Zhang<sup>1,2</sup>,  
4 Manish Raj Gouli<sup>1,2,3</sup>

5 <sup>1</sup>Key Laboratory of Mountain Hazards and Earth Surface Processes, Chinese Academy of Sciences, Chengdu, 610041, China

6 <sup>2</sup>Institute of Mountain Hazards and Environment, Chinese Academy of Sciences, Chengdu, 610041, China

7 <sup>3</sup>University of Chinese Academy of Sciences, Beijing 100049, China

8 <sup>4</sup>Department of Civil and Environmental Engineering, The Hong Kong University of Science and Technology, Clear Water  
9 Bay, Hong Kong, China

10 *Correspondence:* Kaiheng Hu (khhu@imde.ac.cn)

11 **ABSTRACT.** Periglacial debris flows boosted by strong earthquakes or climatic warming in alpine mountains play a crucial  
12 role in ~~delivering~~ sediment ~~delivery~~ from hillslopes and downslope channels into rivers. Rapid and massive sediment supply  
13 to rivers by the debris flows has profoundly influenced the evolution of the alpine landscape. Nonetheless, there is a dearth of  
14 knowledge concerning the roles tectonic and climatic factors played in the intensified sediment erosion and transport~~ation~~. In  
15 order to increase our awareness of the mass wasting processes and glacier changes, five debris flows that occurred at the  
16 Zelunglung catchment of the eastern ~~Himalayan syntaxis of the Himalayas~~ since ~~the~~ 1950 Assam earthquake are investigated  
17 in detail by field surveys and long-term remote sensing interpretation. Long-term seismic and meteorological data indicate that  
18 the four events of 1950-1984 were the legacies of the earthquake, and recent warming events drove the 2020 event. The  
19 transported sediment volume indexed with a non-vegetated area on the alluvial fan reduced by 91% to a stable low level nearly  
20 40 years after 1950. It is reasonable to hypothesize that tectonic and climatic factors alternately drive the sediment supplies  
21 caused by the debris flows. High concentrations of coarse grains, intense erosion, and extreme impact force of the 2020 debris  
22 flow raised concerns about the impacts of such excess sediment inputs on the downstream river evolution and infrastructure  
23 safety. In regard to the hydrometeorological conditions of the main river, the time to evacuate the transported coarse sediments  
24 is approximately two orders of magnitude ~~longer than of~~ the recurrence period of periglacial debris flows.

25 **1 Introduction**

26 Glacier-related hazards are widely developed in alpine regions around the world, such as the Alps, Himalayas, Caucasus,  
27 Tianshan, and Andes (Huggel et al., 2004; Iribarren Anaconda et al., 2015; Petrakov et al., 2007; Richardson and Reynolds,  
28 2000; Shen et al., 2013). These hazards, including ice/rock avalanches, periglacial debris flows, glacial lake outburst floods  
29 (GLOFs), and dammed lakes, have caused ~~substantial huge~~ economic and human losses in the high mountains and their  
30 surrounding area (Bajracharya and Mool, 2009; Hu et al., 2019; Tian et al., 2017; Yu et al., 2021). Especially in the context of

设置了格式: 字体: 10 磅

设置了格式: 字体: 10 磅

climate change (rising temperatures and increased extreme precipitation events), the high-altitude regions such as European mountains, high-mountain Asia, and the Andes are undergoing rapid deglaciation that increases the magnitude and frequency of ice/rock avalanches and low-angle glacier detachments accordingly (Iribarren Anaconda et al., 2015; Krautblatter et al., 2013). Earthquakes, climate warming, geothermal heating, rainfall, and meltwater all directly trigger glacier-related hazards (Haeberli and Whiteman, 2021; Huggel et al., 2004). The Himalayan mountains, which are tectonically active and sensitive to climate change, have experienced many glacier-related disasters triggered by large-magnitude earthquakes or climate warming in recent years. For example, on the 25 April 2015 Gorkha earthquake triggered a catastrophic, a disastrous ice-rock collapse in Nepal's Langtang Valley, causing over 350 casualties~~was triggered by the Gorkha earthquake and killed or left missing at least 350 people in the Langtang Valley of central Nepal~~ (Kargel et al., 2016). Between From 2017 to and 2018, multiple several ice-rock avalanches in the Sedongpu catchment, of Milin County, Tibet Autonomous Region (TAR), China, which triggered large-scale glacial debris flows events that twice dammed~~blocked~~ the Yarlung Tsangpo River ~~twice~~ (Hu et al., 2019; Jia et al., 2019; Li et al., 2022). On 7 February 2021, about  $27 \times 10^6$  m<sup>3</sup> of rock and ice collapsed and quickly transformed into a debris flow in Chamoli, Uttarakhand region of India, which killed more than 200 people and severely damaged two hydropower projects (Shugar et al., 2021). The rising frequency and magnitude of such~~The increased~~ disasters have profound hydrogeomorphic and socio-economic impacts on the high-altitude and surrounding regions, including sediment yield and transportation, alpine landscape evolution, river management, food and water security, hydropower utilization, and infrastructure construction (Evans and Clague, 1994; Kääb et al., 2021), leading to the challenges of transboundary hazards and international collaboration.

Periglacial debris flows ~~triggered~~~~driven~~ by earthquake or climatic events are a major agent of sediment evacuation from steeplands to rivers in high-altitude mountains. ~~These flows result in massive The volume of~~ ice loss and sediment ~~transportation via periglacial debris flows is huge and poses, causing~~ long-term ~~impacts effects on the~~ high mountain environment. The Institute of Mountain Hazards and Environment, Chinese Academy of Sciences (IMHE, CAS) reported that periglacial debris flows in the Guxiang catchment of southeastern Tibet transported a total ~~volume~~ of 200 Mm<sup>3</sup> of sediment ~~transported~~ into an upstream tributary of the Brahmaputra River ~~by periglacial debris flows of the Guxiang catchment in southeastern Tibet between from 1953 to and 1999~~ (Wang et al., 2022). Similarly, The~~the~~ ice-rock avalanches of the Sedongpu in October 2018 delivered approximately about 33.2 Mm<sup>3</sup> of sediment into the Yarlung Tsangpo River (Hu et al., 2019). The total mass loss caused by glacier-rock avalanches in Sedongpu between 2014 and 2018 reached > 70 Mm<sup>3</sup> of glacier and rock and > 150 Mm<sup>3</sup> of moraine deposits (Li et al., 2022). Furthermore, after the glacier detachment of the Sedongpu in 2018, a huge volume of ~335 Mm<sup>3</sup> ~~material~~ was eroded from its glacier bed and transported into the Yarlung Tsangpo (Kääb and Girod, 2023). Such, Sudden sudden, massive~~enormous~~ sediment inputs greatly influence sediment transport capacity, knickpoint formation, river water quality, downstream floods, and delta progradation. For instance, The~~the~~ 2021 Chamoli event resulted in extremely suspended sediment as 80 times high as the permissible level in the Ganga River, ~900 km from the source (Shugar et al., 2021). Sediment fluxes have increased two- to eight-fold in many glacierized and peri-glacierized

设置了格式: 字体: (默认) Times New Roman

批注 [hL1]: L47: Maybe "triggered by" rather than "driven by"?

● Author's response:

Thank you for your suggestion. We agree that "triggered by" is more appropriate in this context. We have revised "driven by" to "triggered by" accordingly.

● Author's changes in manuscript:

We revised "driven by" to "triggered by"

basins between the 1950s and 2010s (Zhang et al., 2022a). Until now, most of previous studies have focused on the residence time and transport of earthquake-triggered landslide sediment at an orogenic scale in no-glacierized environments (Dadson et al., 2004; Dai et al., 2021; Parker et al., 2011; Wang et al., 2015). ~~Little attention has been given to~~ ~~Little attentions are paid on~~ the sediment evacuation progress by post-seismic debris flows at a catchment in glacierized environments owing to relatively low likelihood of debris flows and absence of long-term site-specific data.

In order to investigate the long-term effects of earthquakes on sediment evacuation in a glaciated catchment, the Zelunglung (ZLL) catchment, a tributary of the Yarlung Tsangpo river in southeastern Tibet that has large areas of temperate glaciers and disturbed intensely by the Ms 8.5 earthquake in 1950, is chosen as our study case. The catchment has long-term remote sensing imagery for ~~interpreting interpreting~~ glacier changes and associated debris flows and relatively well-documented records of at least four historical periglacial debris flows in 1950, 1968, 1972, and 1984 since the 1950 Assam earthquake (Zhang and Shen, 2011; Zhang, 1992). The most recent debris-flow event occurred on 10 September 2020, triggered by a small-scale ice-rock avalanche. ~~It is believed that historical earthquakes and ongoing climate warming drove such these events~~ (Bessette-Kirton and Coe, 2020; Deline et al., 2015; Stoffel et al., 2024; Zhang et al., 2022b). Field surveys were carried out before and after the 2020 event, including three ~~periods of~~ aerial photography ~~sessions~~ on 9 September, 11 September 2020, and 21 December 21, 2022, ~~using a with~~ DJI Unmanned Aerial Vehicle (UAV). Dynamic process and sediment characteristics of the 2020 event were examined with the details of aerial photos and field measurements. The ~~Zelunglung's~~ ZLL glacier and alluviation fan changes were interpreted with high-resolution optical remote sensing images from 1969 to 2022. The non-vegetated area of the alluvial fan was used as an index to reflect the variation of sediment supply caused by the periglacial debris flows. ~~By Integrating integrating~~ with historical data ~~of on~~ neighboring earthquakes, temperature, and precipitation, we ~~analyzed demonstrate~~ the trend of periglacial debris flows ~~in over~~ different periods. This case study is helpful for a better understanding of the controlling factors and sediment transportation of periglacial debris flows in High Mountain Asia (HMA).

## 2 Study area

The Zelunglung ZLL catchment (ZLL) (94°56'13.4"E, 29°36'25.6"N) at Zhibai Village in the China's TAR is a tributary on the right bank of the lower Yarlung Tsangpo River, originating from the west side of Namche Barwa massif (7782 m) in the easternmost part of the Himalayas. The main stream flows westward into the Yarlung Tsangpo at an elevation of 2810 m, with a local relief of 4972 m (Fig. 1b). It has a drainage area of 41.21 km<sup>2</sup> with a 17.9 km<sup>2</sup> glacier area. High lateral moraines on both sides of the main glacier divide the drainage network into the main channel, south branch, and north branch (Fig. 1c). The south branch, with a total length of 9.8 km and an average gradient of 275%, originates from the southern cliff at an elevation of ~5900 m. Hanging glaciers on the ridge and freeze-thawing in the cold region make the study area prone to ice and rock avalanches (Fig. 1d).

**批注 [hL2]:** Several of the new sections would benefit from review of the language (e.g.: "Little attentions are paid on" or "imagery for interpreting glacier changes")

● Author's response:

Thank you very much for your valuable comments and suggestions. We have carefully reviewed the language in the new sections and made the necessary corrections.

● Author's changes in manuscript:

We have revised "Little attentions are paid on" to "Little attention is paid to...", and "imagery for interpreting glacier changes" to "imagery for interpreting glacier changes".

We have made the necessary corrections in other sections.

**批注 [hL3]:** Several of the new sections would benefit from review of the language (e.g.: "Little attentions are paid on" or "imagery for interpreting glacier changes")

● Author's response:

Thank you very much for your valuable comments and suggestions. We have carefully reviewed the language in the new sections and made the necessary corrections.

● Author's changes in manuscript:

We have revised "Little attentions are paid on" to "Little attention is paid to...", and "imagery for interpreting glacier changes" to "imagery for interpreting glacier changes".

**批注 [hL4]:** L71: "It is believed that historical earthquakes and ongoing climate warming drove these events" needs a citation or justification. Who believes that?

● Author's response:

Thank you for your suggestion. The driving factors behind the historical debris flow events in the ZLL catchment require further discussion in this manuscript. Therefore, we have revised "these events" to "such events" for greater precision. Additionally, we have included references to studies of similar hazards in other regions worldwide at the end of this sentence to provide proper justification.

● Author's changes in manuscript:

we revised the sentence as follows:

It is believed that historical earthquakes and ongoing climate warming drove such events (Bessette-Kirton and Coe, 2020; Deline et al., 2015; Stoffel et al., 2024; Zhang et al., 2022).

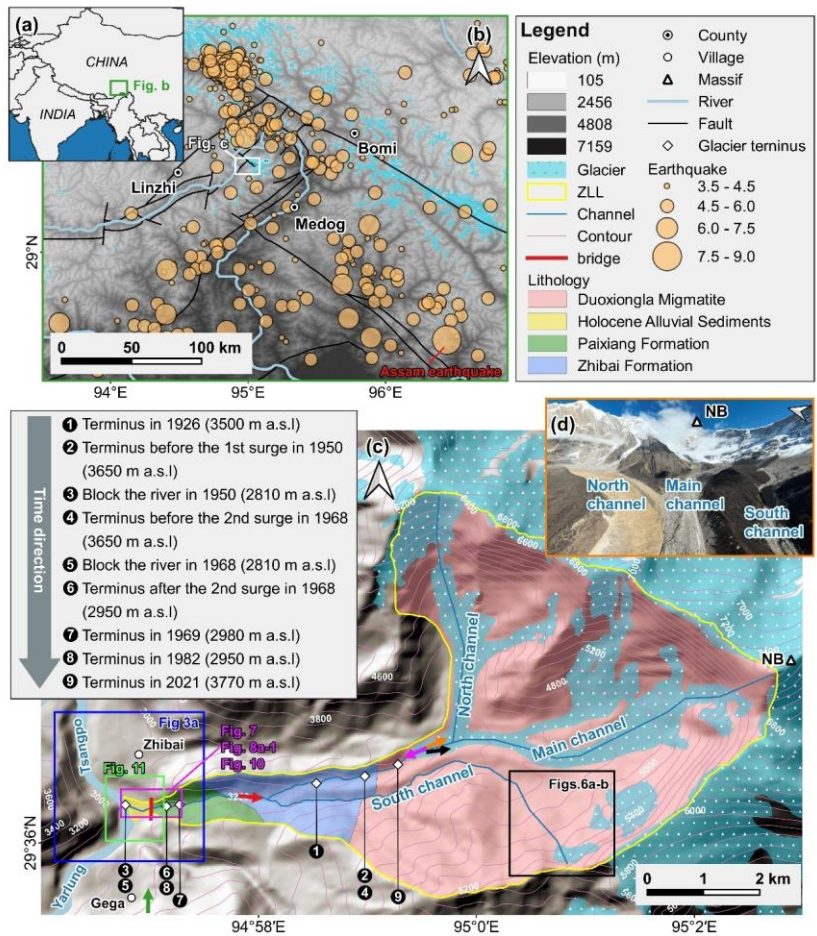
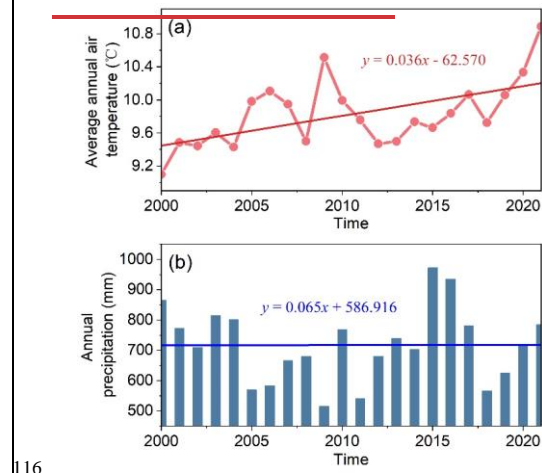


Figure 1: (a) Regional overview map of southeastern Tibet. (b) Regional settings and historical earthquakes of southeastern Tibet. (c) Topographic, geological and glacier terminus change maps of the Zelunglung catchment (the lithology refers to (Zhang and Shen, 2011)). The orange, rose-red, green, black and red coloured arrows represent the view angle direction of figures 1d, 4, 5, 6c and 6d. (d) Aerial photo of the Zelunglung glacier and channels on December 21, 2022 (NB denotes the Namche Barwa massif).

The regional tectonic units are the Lhasa terrane, the Indus-Yarlung Tsangpo suture, and the eastern syntaxis of the Himalayas from north to south (Hu et al., 2021). The catchment lies in the eastern syntaxis, which is uplifting at a rate of 5-10

101 mm/a (Ding et al., 2001). The exposed stratum in the Zelunglung-ZLL is known as the Namche Barwa Group complex, which  
 102 is composed of Duoxiongla migmatite, Zhibai group, and Paixiang group gneiss. The Quaternary deposits consist of Holocene  
 103 alluvium at its outlet, thick layers of glacial till, and glacio-fluvial accumulation, especially hundreds of meters of huge thick  
 104 moraine layers with large boulders accumulated on both sides of the main channel (**Fig. 1c**) (Han and Feng, 2018; Zhang and  
 105 Shen, 2011). Many active faults are distributed around the study area, such as the Aniqiao-Medog Fault to the east, which is  
 106 considered the seismogenic fault of the 1950 Ms=8.5 Assam earthquake, NW-SE Xixingla fault that is the seismogenic fault  
 107 of the 2017 Ms=6.9 Milin earthquake, and Daduka Fault across the Zelunglung-ZLL downstream (Hu et al., 2019). Neotectonic  
 108 movement makes this area highly susceptible to intense and frequent earthquakes.

109 This catchment lies in the rain shadow area of Mt. Namche Barwa, and its precipitation is controlled by the Indian Ocean's  
 110 humid monsoon through the Yarlung Tsangpo Gorge. The climate has a strong vertical difference: semi-humid climate zone  
 111 beneath 3200 m, cold temperate climate zone between 3200-4000 m, and cold climate zone above 4000 m. According to the  
 112 data recorded at the Linzhi meteorological station 46.2 km west of the Zelunglung-ZLL, the annual air temperature with a mean  
 113 value of 9.8 °C increases at an average rate of 0.36 °C/10a from 2000 to 2021, which is much higher than the global average  
 114 (Chen et al., 2015). Meanwhile, the annual precipitation ranges from 514 mm to 972 mm, exhibiting notable inter-annual  
 115 variation, with no distinct trend over the past 20 years and increases at an average rate of 0.65 mm/10a (Fig. 2).



116

**批注 [hL5]:** L129: As I said before, I do not see an increase in precipitation rates here. The increase is so small it must surely be within the uncertainty of the scatter of the data. If you plotted the confidence bands of the regression or added the standard error of the slope of the line, I would bet it is way within uncertainty of 0 or a decreasing trend. Also, in the discussion, you say there is no significant trend in precipitation.

**● Author's response:**  
 We sincerely thank the Reviewer for their careful review. We agree with the Reviewer's point that the observed increase in precipitation rates may fall within the uncertainty range of the data. As suggested, we have re-analyzed the data by calculating the standard error of the slope (Fig. 2). The results show that the slope value is 0.065, the standard error is 4.215. The t-statistic value is approximately 0.0153, which is much smaller than the critical t-value of 2.086 at the significance level of  $\alpha=0.05$ . This indicates that the trend is not statistically significant. In the revised manuscript, we have clarified that there is no significant trend in precipitation over the study period, aligning the discussion with the updated statistical analysis.

**● Author's changes in manuscript:**  
 We have replaced Figure 2 with Figure SS, and changed the L109 as: The annual precipitation ranges from 514 mm to 972 mm, exhibiting notable inter-annual variation, with no distinct trend over the past 20 years

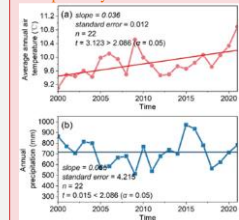


**Figure 2: Annual temperature and precipitation data from 2000 to 2021 at Linzhi Meteorological Station (Data source: <https://www.ncei.noaa.gov/maps/annual/>).**

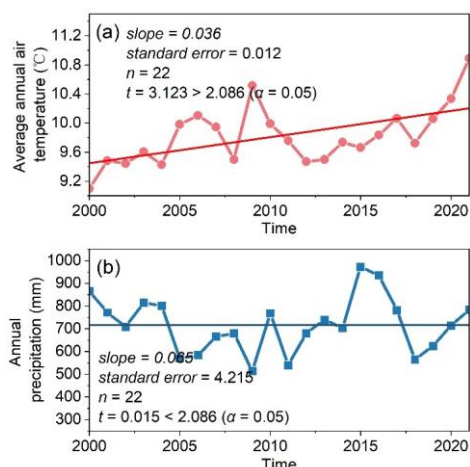


**Figure 2: Annual temperature and precipitation data from 2000 to 2021 at Linzhi Meteorological Station. (Data source: <https://www.ncei.noaa.gov/maps/annual/>).**

The ZLL basincatchment, characterized bywith its unique geographical and climatic conditions, has hosted been a cradle for the extensive glaciation proliferation of glaciers and a hotbed of frequent glacial activity throughout over geological time. The Zelunglung-ZLL has experienced at least three glaciations in the Last Glacial Maximum (LGM), Neoglaciation, and Late Holocene (Hu et al., 2020). The LGM moraine extended into the Yarlung Tsangpo and dammed the river (Huang et al., 2014; Liu et al., 2006; Montgomery et al., 2004; Zhu et al., 2012). The glacier surges/debris flows - dammed lake - outburst flood disaster events since the last glacial period also had an important impact on the landform and paleogeographical environment of the Yarlung Tsangpo Valley (Wang et al., 2021). The modern glaciers in this area are strongly influenced by the Indian monsoon and are highly sensitive to climate change. Hence, the Zelunglung-ZLL glacier has advanced and retreated many times since the last century. The high instability and rapid changes of the glacier result in several glacier surges or calving events. As shown in Fig. 1c, the glacier snout was 3500 m a.s.l in 1926 (Ward, 1926). Since the 1950s, the Zelunglung-ZLL glacier has experienced three surges or rapid advances (Zhang, 1985, 1992). The first surge occurred on August 15, 1950. Following the 1950 Assam earthquake, the terminus of Zelunglung-ZLL Glacier advanced from 3650 m a.s.l to the Yarlung Tsangpo at 2810 m a.s.l with a horizontal displacement of up to 4.5 km. This event destroyed the Zhibai Village completely at the mouth of the Zhibai gully, killed 98 people, and formed an ice dam as high as tens of meters in the main river. The second surge occurred one afternoon in August or September of 1968 (corresponding to July 1968, in Tibetan calendar) when it was sunny (Zhang, 1985, 1992). The advance also resulted in a temporary ice dam in the Yarlung Tsangpo and deposited a glacial boulder of 4.0×5.0×5.5 m upstream of the dam (Zhang, 1985). It is worth noting that the position of the ice tongue

设置了格式: 字体: (中文) + 中文正文 (宋体), (中文) 简体中文 (中国大陆)

设置了格式: 非突出显示



137 before the second glacier surge has returned to the position before the first surge (3650 m a.s.l), and the ~~peak velocity~~highest  
138 ~~speed of these the two glacier~~ surges ~~reached was up to~~ 1.5 km/d. After the second surge, the main glacier split into 6 segments  
139 due to differential ablation, and the terminus of the lowest segment of the glacier was at 2950 m a.s.l. The terminus of the  
140 lowest segment was about 2980 m a.s.l in 1969 as shown by the Corona reconnaissance satellite images (Kääb et al., 2021).  
141 The terminus of the lowest part of the glacier had probably been at 2950 m a.s.l before 13 April 1984 when an ice mass of  
142 80000 m<sup>3</sup> detached at 3700 m a.s.l and traveled horizontally 150 m, which was the third rapid advance of the Zelunglung ZLL  
143 glacier (Zhang, 1992). After that, no glacier surges or detachments were recorded, but small-scale mountain torrents or debris  
144 flows occurred almost yearly (Zhang and Shen, 2011). At present, the glacier terminus is about 3770 m a.s.l.

145 **3 Data and methodology**

146 **3.1 Data sources**

147 We collected a total of 30 different remote sensing images from various sources dating back to 1969, with resolutions ranging  
148 from 1m to 15m (**Table 1**). The ~~1969~~-Keyhole ~~image refers to Kääb et al. (2021) and the other~~ images before 1982 were  
149 sourced from the Keyhole reconnaissance satellites (<https://earthexplorer.usgs.gov/>), originally serving as the primary data  
150 source for the United States Department of Defence and intelligence agencies for Earth imaging. These high-resolution images  
151 provide valuable visible data in the era without commercial satellite imagery. Images from 1988 to 2007 originated from the  
152 Centre National d’Études Spatiales (CNES) SPOT series data (<https://regards.cnes.fr/user/swh/modules/60>). Images from 2009  
153 are sourced from the RapidEye series and Planet satellites (<https://account.planet.com/>), which are known for their short revisit  
154 periods and high resolution. To comprehensively document the historical debris flow activity in Zelunglung ZLL, we diligently  
155 chose images captured after every rainy season (October to December) whenever feasible. Due to high cloud cover in the study  
156 area and limited availability of image resources, we substituted images from the following year before May for specific periods  
157 with significant image data gaps (e.g., before 2000) for those of the missing year (Li et al., 2017). Although the Landsat satellite  
158 series may offer more continuous observational records, their relatively coarse resolution makes them unsuitable for our study  
159 area.

160 **Table 1: Data sources of the satellite images used in this study.**

No.	Date	Data sources	Resolution (m)
1	1969/ <u>12/08</u>	Keyhole	<u>51</u>
2	1972/2/28	Keyhole	1
3	1973/3/26	Keyhole	1
4	1975/12/21	Keyhole	4
5	1979/4/10	Keyhole	1
6	1982/10/15	Keyhole	1

7	1988/2/20	Spot1	15
8	1989/12/1	Spot1	15
9	1990/12/21	Spot2	12
10	1991/11/25	Spot3	12
11	2000/11/17	Spot4	10
12	2002/12/5	Spot5	6
13	2004/12/28	Spot5	6
14	2005/10/10	Spot5	6
15	2006/12/21	Spot5	6
16	2007/11/29	Spot5	6
17	2009/12/22	RapidEye	5
18	2010/12/15	RapidEye	5
19	2011/11/23	RapidEye	5
20	2012/12/15	RapidEye	5
21	2013/12/7	RapidEye	5
22	2014/12/13	RapidEye	5
23	2015/12/6	RapidEye	5
24	2016/12/13	Planet	3
25	2017/12/11	Planet	5
26	2018/12/13	Planet	3
27	2019/12/7	Planet	3
28	2020/12/10	Planet	3
29	2021/12/12	Planet	3
30	2022/12/10	Planet	3

3.2 Methodology

This study ~~combines~~utilizes a combination of field surveys, aerial drone photography, and satellite imagery analysis to investigate debris flow events in the ~~Zelunglung-ZLL region~~catchment. The ~~h~~Historical records of the four debris flows ~~lack~~have no volume data. High-resolution orthoimages and digital surface models are generated to assess terrain changes, while non-vegetated area (NVA) serves as a proxy for sediment volume for time series ~~analysis~~analyses. The integration of these methods ~~provides~~offers a detailed insight into the debris flow history and its influencing factors.



### 167 3.2.1 Field surveys

168 We conducted three field surveys in the Zelunglung-ZLL between 2020 - 2022. During the initial two survey, we conducted  
169 two aerial drone photography works on September 9 and 11, 2020, using DJI MAVIC 2. Additionally, we measured  
170 downstream channel cross-sectional morphology, debris flow particle characteristics, and the extent of damage to the Zhibai  
171 Bridge, and sampled debris flow materials with size < 100 mm on the accumulation fan in the second survey. A full 3D view  
172 of the Zelunglung-ZLL was captured with an unmanned aerial vehicle (UAV) in the third survey on December 21, 2022, a  
173 sunny winter day (**Fig. 1d**).

### 174 3.2.2 NVA interpretation

175 The inundation of debris flow on the alluvial fan often destroys vegetation cover and causes the affected area desertification  
176 in a few years. Generally, the ~~non-vegetated-area-NVA~~ depends on the flow magnitude. So, the NVA~~non-vegetated-area~~ of the  
177 alluvial fan shortly after a glacial debris flow can serve as a proxy of the volume of transported sediment. It should be noted  
178 that distinguishing fresh debris flow deposits on an alluvial fan from pre-existing exposed surfaces in the surrounding area is  
179 challenging in satellite images due to minimal color differences. ~~Additionally, due to the slow vegetation recovery rate in high-~~  
180 ~~altitude regions, our interpretation area likely includes exposed areas one year or several years before an event.~~ Therefore, the  
181 NVA has some uncertainties in representing the real magnitude of the debris flows.

182 We employed a visual interpretation approach to delineate ~~NVA~~non-vegetated areas within the Zelunglung's-ZLL alluvial  
183 fan. Identifying the NVA~~non-vegetated-area~~ is primarily based on differences in color, hue, texture, and shading between  
184 vegetated and unvegetated regions. The Keyhole black and white photos and the SPOT single-band black and white images  
185 show distinct tonal differences between vegetated and unvegetated areas. In the true-color images obtained from RapidEye  
186 and Planet, the boundaries of NVAs are highly conspicuous. The Zelunglung-ZLL interpretation zone is limited to the region  
187 between the two adjacent confluences of its upstream and downstream catchments with the main river.

188 Due to potential misalignment between remote sensing images from different sources, image matching is performed before  
189 manual delineation of the ~~NVA~~non-vegetated areas (Cui et al., 2022). To eliminate the errors of geospatial locations of the  
190 images from different sources, we used the 2020 Planet image as the reference image and selected ground control points with  
191 clear markers on this image, such as road junctions, rivers, and typical topographic points. Third-order polynomial  
192 transformation is applied to match the images from other sources accurately with the 2020 image, ensuring a positional error  
193 of less than 20 m relative to the reference image. The original Keyhole images without geographical coordinates and projection  
194 system information are georeferenced with the 2020 Planet image with the ground control points. We assume that the visual  
195 interpretation error of ~~NVA~~non-vegetated areas is approximately one grid cell on either side of the boundary. Moreover, we  
196 verified the interpretation results of the remote sensing images with the UAV orthoimages.

197 3.2.3 Drone image interpretation

198 We employed Pix4DMapper and Arcmap10.8 to ~~generatedeal with~~ the UAV digital orthophoto maps (DOMs) and digital  
199 surface models (DSMs), ~~as well as to perform generation and~~ DSMs differencing. ~~Since we did not deploy~~As ground control  
200 points (GCPs) ~~were not deployed~~ during drone photography, we generated ~~the~~ DSM and DOM ~~of for~~ September 9 in  
201 Pix4DMapper-. ~~Subsequently, and then selected~~ 20 relatively stable points, ~~that were not un~~affected by debris flow events,  
202 ~~were selected~~ as GCPs in Arcmap ~~using the September 9with~~ DOM ~~of September 9~~ as a reference. These control points were  
203 then ~~applied used~~ in Pix4DMapper to generate the ~~September 11~~ DSM and DOM ~~for September 11~~. Then ~~the~~ DSMs of  
204 difference (DoD) ~~analysis differencing~~ was ~~subsequently~~ conducted in Arcmap. To determine the uncertainty ~~for in~~ our DoD  
205 differencing result we follow methods outlined in Shugar et al. (2021). ~~We identified a series of fifteen~~ Fifteen stable areas on  
206 old debris flow terraces adjacent to the valley floor-~~Mainly, mainly~~ roads and unseeded farmlands, ~~were identified.~~ )~~and~~  
207 ~~retrieved the~~ The standard deviation of DoD values within these areas ~~was calculated~~ and used ~~these~~ to estimate a two-sigma  
208 DoD uncertainty. ~~The resulting uncertainty was estimated to be~~ The uncertainty was  $\pm 0.493$  m.  
209 Utilizing post-event DOM captured on September 11, we visually interpreted the distribution of particles from the downstream  
210 channel to the depositional fan on Arcmap10.8. High resolution and accurate color representation of the drone aerial images  
211 enable us to reliably identify coarse particles (>50 cm). The interpretation results were compared with measurements obtained  
212 with a caliper during the 2022 field survey.

213 4 Debris-flow events and Sediment characteristics

214 4.1 Multi-periodic glacial debris flows

215 Glacier surges or ice-rock avalanches can be transformed into debris flows that deliver massive amounts of sediment into the  
216 river or deposit on the alluvial fan. Four large-magnitude debris flows accompanied by glacier instability occurred in 1950,  
217 1968, 1973, and 1984 (Zhang, 1992; ~~Peng et al., 2022~~). ~~The 1968 event coused significant deposition in the alluvial fan,~~  
218 ~~characterized by a rough surface and indistinct channels (Fig. 3-a2).~~ ~~The magnitude of the 1950 event is perhaps more~~  
219 ~~significant than that of the 1968 event. According to Zhang (1992), the detached glacier in 1950 climbed over the ~80 meters~~  
220 ~~lateral moraine on the north at an elevation 4000 m and traveled downstream along the Zhibai gully (Fig. 1e3-a1 and Fig. 4).~~  
221 ~~Based on the erosional scar photo on the lateral moraine (Zhang, 1992) and the 2022 UAV photo, the residual depositional~~  
222 ~~area of the 1950 event in the upstream gully is ~ 65,000 m<sup>2</sup> (Fig. 4). Although the glacier detachment happened in~~  
223 ~~ZelunglungZLL in 1950, most of the sediment deposited in the Zhibai channel and its alluvial fan. Fine sediment from the~~  
224 ~~catchment can be quickly transported downstream by river flows, but most coarse sediment is still left on the bank or the~~  
225 ~~alluvial fans. There are two terraces on the banks of the main river along the confluences of the ZelunglungZLL~~  
226 ~~ravinecatchment and Zhibai gully (Fig. 5a). T1 and T2 terraces are ~10 m and ~ 150 m above the river level, respectively (Fig.~~  
227 ~~5b). The 1950 and 1968 events completely dammed the Yarlung Tsangpo (Zhang, 1992). Compared with the 1969 Keyhole~~

设置了格式: 字体颜色: 红色

批注 [hL6]: We have adjusted the statement logic in Section 4.1, and added more details about the fan surface, channel and glacier changes in-between the major debris flows. The major debris flows in the 40 years after the 1950 earthquake were all associated with trunk glacier disturbances caused by the earthquake, which answered the questions of reviewers 1 and 2.

设置了格式: 字体: 加粗

设置了格式: 字体: 加粗

228 image (Fig. 3a), it is likely that the T1 terrace is the residual dam of the 1968 event. The debris flows in the 1950 glacier surge  
229 event eroded the T2 terrace (Fig. 3-a2), which implies that the T2 terrace formed before 1950. The residual inundation area of  
230 the 1950 event is ~0.78 km<sup>2</sup> (Fig. 5a). If the magnitude is proportional to the inundation area, the flow magnitude of the 1950  
231 event could be larger than that of the 1968 event.  
232 From the 1972 and 1973 images, it is observed that fresh debris deposits inundated the north part of the fan and did not go  
233 beyond the 1968 accumulation zone (Fig. 3-a2, 3-b2 and 3-c2). The same lobes and deposition boundary and the marked  
234 collapse of the terminal glacier (Fig. 3-b3 and 3-c3) indicate that the so-called 1973 event mentioned by Peng et al. (2022)  
235 likely happened in 1972. The fan in December 1975 exhibits significant brightness variations (Fig. 3-d2), with pronounced  
236 channelization above the glacier (Fig. 3-d1), indicating possible debris flow activity prior to this time. Compared with 1975,  
237 the fan in 1979 displays a flatter terrain and more distinct channelization (Fig. 3-e2), indicating the modification of the rough  
238 fan surface by debris flow activity. This also implies that, due to limited information at the time, additional events during this  
239 period may have gone unrecorded. By 1982, noticeable vegetation had recovered in the middle part of the fan (Fig. 3-f2).  
240 Concurrently, accelerated glacier ablation exposed lateral moraines (Fig. 3-e3 and 3-f3), while the glacier terminus developed  
241 an extensive crevasse network (Fig. 3-f4 and 3-f5). These fractured ice bodies and moraine materials, under the impact of ice  
242 avalanche at 3700 m described by Zhang (1992), contributed to the formation of the 1984 large-scale debris flow. The  
243 magnitude of the 1950 event is perhaps more significant than that of the 1968 event. According to Zhang (1992), the detached  
244 glacier in 1950 climbed over the ~80 meters lateral moraine on the north at an elevation 4000 m and traveled downstream  
245 along the Zhibai gully (Fig. 1c and Fig. 4). Based on the erosional scar photo on the lateral moraine (Zhang, 1992) and the  
246 2022 UAV photo, the residual depositional area of the 1950 event in the upstream gully is ~65,000 m<sup>2</sup> (Fig. 4). Although the  
247 glacier detachment happened in Zelunglung in 1950, most of the sediment deposited in the Zhibai channel and its alluvial fan.  
248 Fine sediment from the catchment can be quickly transported downstream by river flows, but most coarse sediment is still left  
249 on the bank or the alluvial fans.

设置了格式; 字体: 加粗

设置了格式; 字体: 加粗

设置了格式; 字体: 加粗

设置了格式; 字体: 加粗

设置了格式; 字体: 加粗

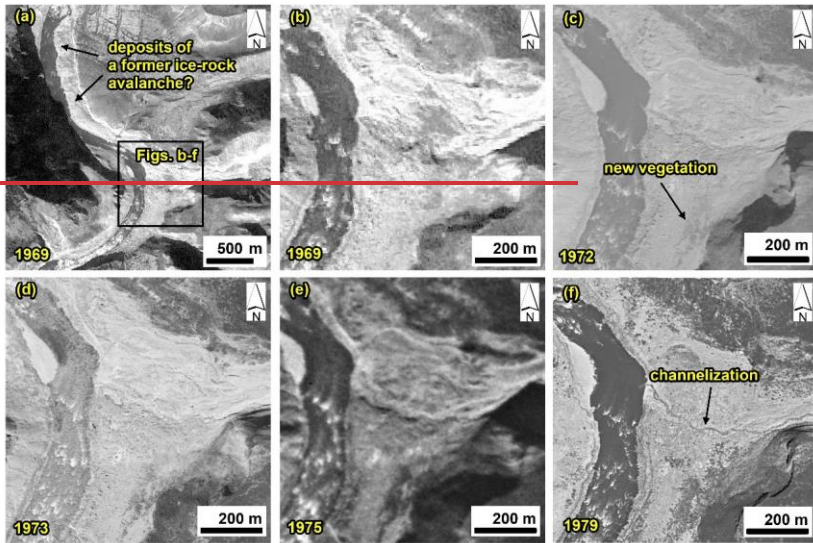
设置了格式; 字体: 加粗

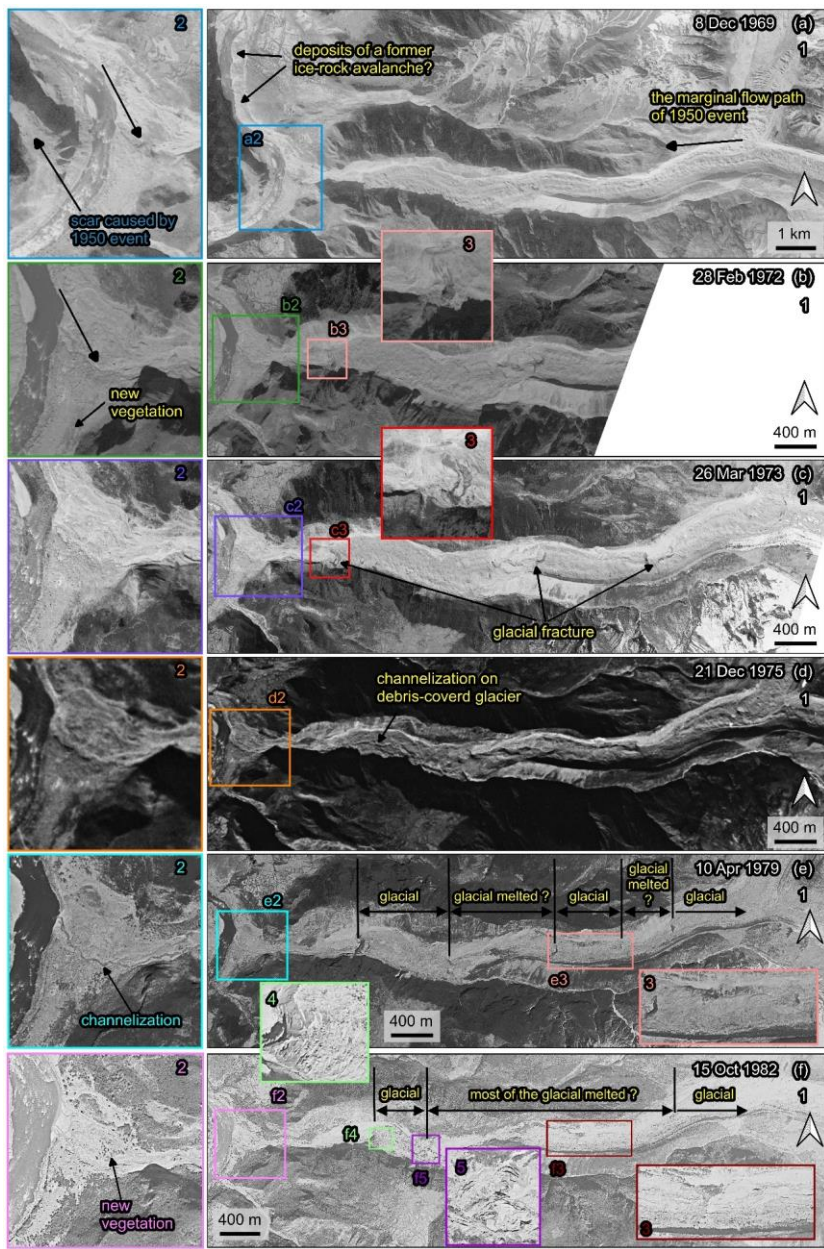
设置了格式; 字体: 加粗

设置了格式; 字体: 加粗

设置了格式; 字体: 加粗

设置了格式; 字体: 加粗







252 **Figure 3: Variations of the Zelunglung alluvial fan and channel during 1969 – 1979/1982.** The images are taken from Keyhole  
253 reconnaissance satellites (<https://earthexplorer.usgs.gov/>).

254 There are two terraces on the banks of the main river along the confluences of the Zelunglung ravine and Zhibai gully (Fig.  
255 5a). T1 and T2 terraces are 10 m and 150 m above the river level, respectively (Fig. 5b). The 1950 and 1968 events  
256 completely dammed the Yarlung Tsangpo (Zhang, 1992). Compared with the 1969 Keyhole image (Fig. 3a), it is likely that  
257 the T1 terrace is the residual dam of the 1968 event. The debris flows in the 1950 glacier surge event eroded the T2 terrace,  
258 which implies that the T2 terrace formed before 1950. The residual inundation area of the 1950 event is 0.78 km<sup>2</sup> (Fig. 5a).  
259 If the magnitude is proportional to the inundation area, the flow magnitude of the 1950 event could be larger than that of the  
260 1968 event.



261 **Figure 4: Aerial photo of the Zelunglung main channel on December 21, 2022, and the old deposits in Zhibai gully left by the 1950**  
262 **event (the view angle direction is denoted by green arrow in figure 1c, and the dashed rectangle indicates the location of Figure 5b).**  
263

批注 [hL7]: We replaced Figure 3 to show more details

- 设置了格式: 字体颜色: 自动设置
- 设置了格式: 字体: 加粗, 字体颜色: 自动设置
- 设置了格式: 字体颜色: 自动设置



Figure 5: Two terraces on the banks of the main river. (a) Century Space's satellite image on 9 February 2021. (b) Picture of the terraces on the opposite bank of the Zelunglung taken on 8 September 2020. (T1 and T2 represent the terraces formed in two different periods. The green arrow denotes the view angle direction of figure b)

An ice-rock avalanche triggered the recently documented glacial debris flow on Sep. 10, 2020. The 2020 ice-rock avalanche initiated on the top ridge of the south branch at an elevation of 5500 m. The scar area of initiated ice and rock was  $1.35 \times 10^4 \text{ m}^2$  on the upper cliff (Figs. 6a-b). The initiated volume is estimated to be  $7.0 \times 10^4 \text{ m}^3$  by using the bedrock landslide area-volume empirical relationship ( $V = \alpha A^\gamma$ ;  $\alpha = 0.186$ ,  $\gamma = 1.35$ ) (Larsen et al., 2010). In the Google image on December 4, 2017 (Fig. 6-c2), it can be seen that there is a protruding rock mass on the cliff below the unstable ice-rock block. The rock mass develops many lateral cracks, and the top is covered with fresh, weathered materials, indicating freezing severe weathering. The fallen ice-rock block partially disintegrated and impacted colluvial deposits on steep hillslope below the cliff at elevations 4570–4800 m, forming a muddy fresh area of  $0.134 \text{ km}^2$  (Fig. 6b). This area is often covered by snow and ice, and the ice-snow melting water easily infiltrates into the debris-ice mixtures. Once the slope material was entrained into the mass flow, such a nearly saturated mixture could quickly turn into a debris flow. Peng et al. (2022) estimated a debris loss of  $1.14 \text{ Mm}^3$  in the scarp area except for the initiated ice and rock. But they mistake the hillslope below the cliff as the source area of the event. It is noted that there is an ice-rock residual of  $\sim 7.14 \times 10^3 \text{ m}^3$  left under the cliff (Fig. 6-b3). That means the volume of the debris mass flowed downward into the south channel should include half of the initiated ice-rock mass and the debris loss of  $1.14 \text{ Mm}^3$ . The entrained volume is at least 16 times the initiated volume.



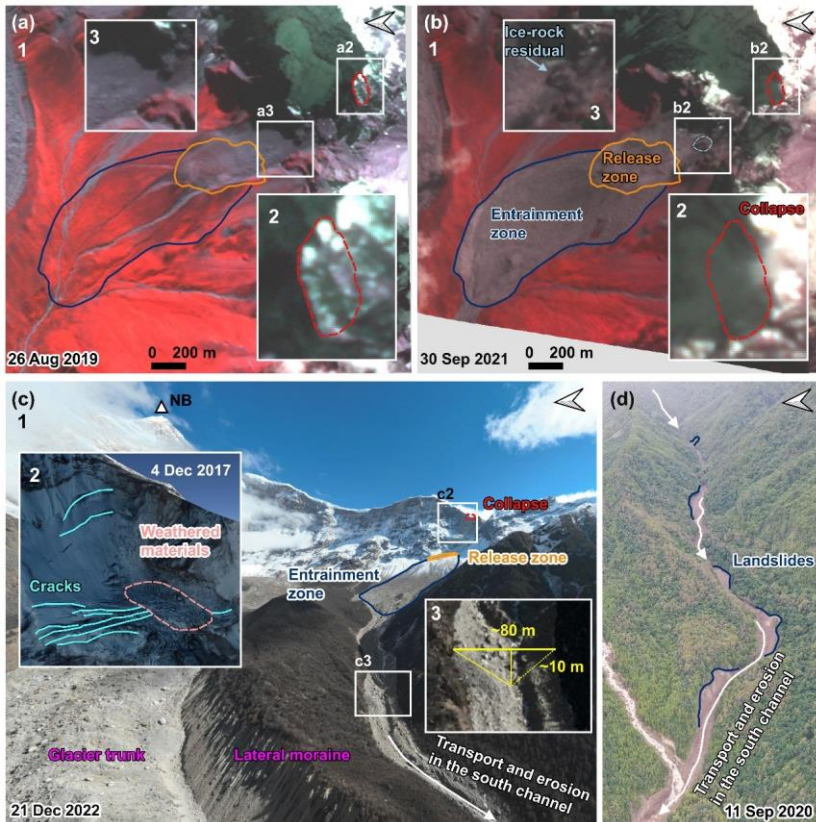


Figure 6: The initiation and propagation of the “9-10-2020” Zelunglung periglacial glacier debris flow. (a) The planet image of the initiation area before the event. (a2) enlarged region over the pre-collapse site. (a3) Enlarge the region over the hillslope before the collapse. (b) The planet image of the initiation area after the event. (b2) enlarged region over the post-collapse site. (b3) enlarged region over the hillslope after the collapse. (base data of a-b: © 2024 Planet Labs PBC) (c) An aerial photo of the source area and the south channel on 21 December 2022 was taken by the UAV. (c2) Google Earth imagery of the initiation area on 2 December 2017 (base data: ©Google Earth). (c3) The region was enlarged over the south channel on 21 December 2022. (d) An aerial photo of the downstream channel on 11 September 2020 was taken by the UAV.

When the debris flows traveled downstream, parts of old channel sediment and lateral moraines were eroded while some of the flow mass was deposited on the banks. The flows also triggered many small landslides on both banks of the middle stream (Fig. 6d). The blockage by large boulders and the induced landslides on the narrow channel may enlarge the magnitude of the debris flows in the end (Fig. 6d) (Cui et al., 2013; Liu et al., 2020). The UAV photo shows the influx of debris flows that

transformed from the entrained sediment and melting water exceeded the average water level of the south channel. The flow cross-section is ~ 80 m wide at the top and ~ 10 m high in the thalweg based on the UAV photo and OpenCycle topographic map (**Fig. 6-c3**). The peak discharge and frontal flow velocity reached 4700 m<sup>3</sup>/s and 11.4 m/s at the outlet (Peng et al., 2022). According to the description of local villagers, the first debris flow surge arrived at Zelunglung's ZLL mouth-outlet at about 5:00 pm on September 10, and the second larger one arrived about one hour later. Two ice-rock avalanches with different volumes probably happened on the ridge and were the corresponding trigger of the downstream debris-flow surges. But it is more likely that there was only one ice-rock avalanche during the event, but a synchronization of the ice-rock impacts in the scarp area, and the channel blockage caused two debris-flow surges.

## 4.2 Sediment characteristics of the 2020 event

### 4.2.1 Difference between the initiation and the downstream areas

Periglacial debris flows can transport rocks or boulders not only in midstream steep channels but also in gentle downstream channels or alluvial fans. The sediment transportation capacity of the flows depends on flow hydrodynamics, grain composition, and topographic conditions. The 2020 Zelunglung-ZLL event provides first-hand information for examining such sediment characteristics of the flows. Next, we present on-site data such as the size distribution of coarse grains, their impact, and erosion. The field evidence shows some features of periglacial debris-flow transportation that differ from fluvial transport.

There is a big difference between the sediment composition in the source and depositional areas. The initiated ice-rock debris and colluvial deposits on steep hillslopes consisted of angular rocks of various sizes. However, we observe that the deposits in the downstream areas are sub-rounded stones, and the downstream banks and channel bed are composed of sands and boulders up to several meters in diameter (**Fig. 7**). That means most of the angular rocks resided in the upslope or upstream channel and did not move downward. The angularity of the fragmented rocks reduced their mobility, and the attenuated overland flow had less transport capacity. The large sub-rounded or sub-angular boulders in the lower reaches came from the middle of the downstream reaches. We guess that grain segregation happened initially, and only fine parts of the ice-rock mass and melting water traveled downward the midstream. The resident angular rocks would be rounded gradually by the periglacial stream and transported downward by the subsequent floods or debris flows. The transportation mode of coarse grains is a kind of “Relay-race style”, one event by one event.

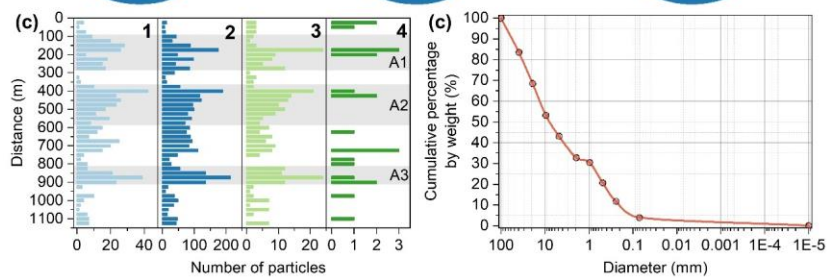
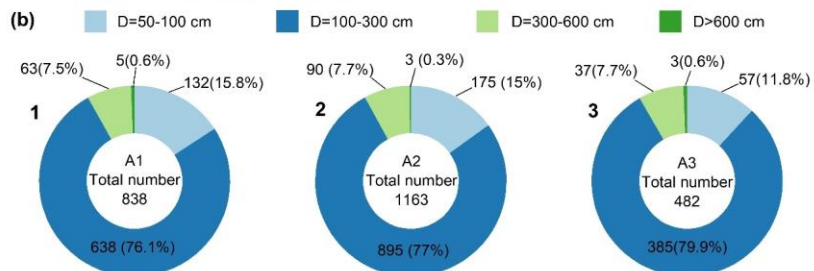
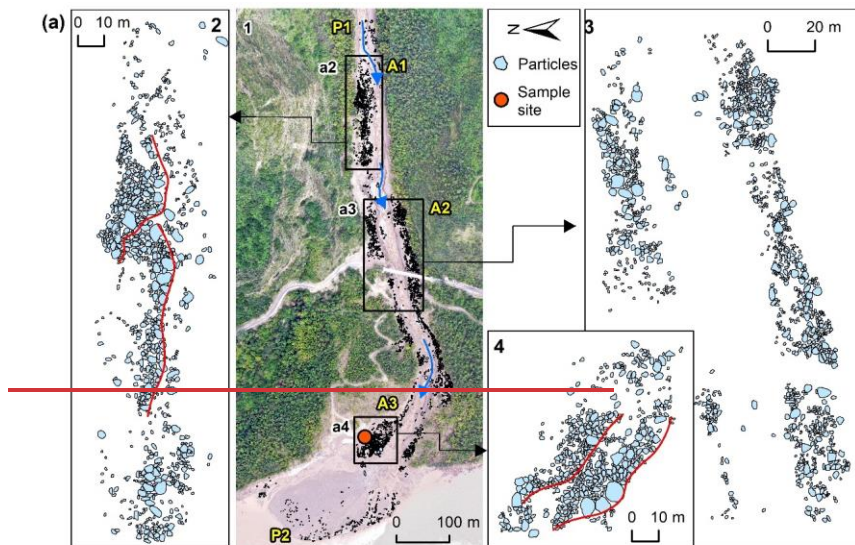
Numerous boulders were on the channel and banks before the 2020 event, as seen from the aerial photo on 9 September 2020 (**Fig. 7a**). The in situ boulders were mobilized by the upstream flows and reorganized spatially. The boulders were prone to move together on the flat banks such as a flat storage yard near the bridge and the fan middle (**Fig. 7b**). The slope and flow depth are critical for the boulder's transport. Interstitial slurry among the boulders could separate from the boulders when the debris flows moved on a gentle slope or spread over an open fan (**Fig. 7c**). The interstitial slurry provided buoyancy for the boulders and reduced resistance between them and the bed. Once there was no interstitial slurry, the boulders quickly stopped.



Figure 7: Comparison of pre-and post-event aerial photos on the downstream channel and alluvial fan. (a) the UAV photo on 9 September 2020; (b) the UAV photo on 11 September 2020; (c) On-site picture of the boulder clustering on 11 September 2020 (the camera angle direction is denoted by red arrow in figure b).

#### 4.2.2 Grain-size distribution of coarse particles > 50 cm

In the downstream channel, with an average gradient of 13.8%, a relatively high velocity (11.4 m/s) enabled the flows to mobilize boulders of 5.0 meters in diameter (Costa, 1983). An 1125 m long straight reach from the first bend upstream of the bridge to the edge of the alluvial fan was chosen. Coarse particles > 50 cm on the deposition surface were visually interpreted from the orthophotos with a resolution of 0.17 m on September 11, 2020, after the debris-flow event. The long axis of the equivalent ellipse of these particles represents the particle size. Due to the limitation of resolution, only coarse particles with a long axis larger than 50 cm were counted (Fig. 8). A total of 3943 coarse particles were identified and divided into four size ranges of 50-100, 100-300, 300-600 and >600 cm. Spatial statistics of these particles were made every 25 m along the central flow line, and then 45 segments were divided.





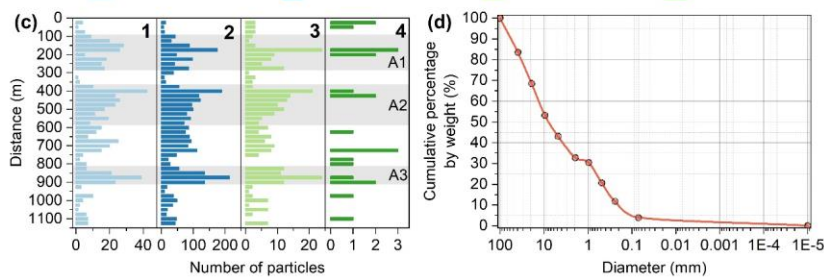
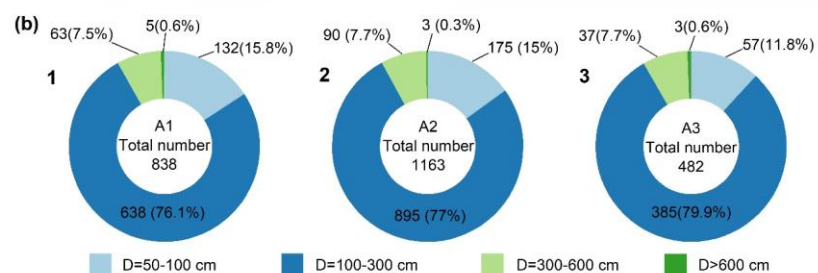
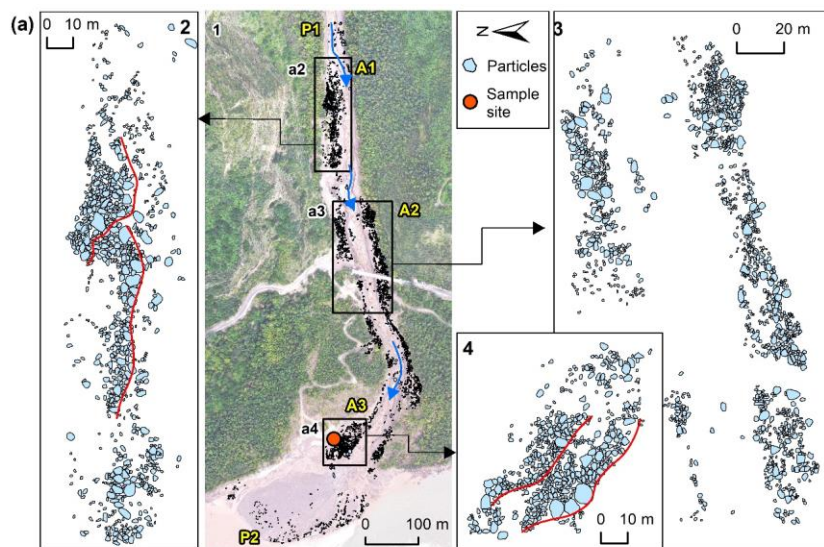


**Figure 8: Distribution of the grain size.** (a) The distribution of coarse particles along the channel and alluvial fan. P1 and P2 represent the places where the count starts and ends, respectively. A1-A3 are the three main deposition sites. The blue arrow is the direction of the debris flows. The bottom image is an orthographic image taken by a drone on September 10, 2020. The locations of the enlarged regions (a2)-(a4) are shown as black boxes. (a2)-(a4) enlarged region over the three main deposition sites A1-A3. Panels (b1)-(b3) show the counts of four groups of the particles in the three main deposition sites A1-A3. Panels (c1)-(c4) show the counts of four groups of the particles in the 45 segments along the channel from P1 to P2. Particles with diameters of 50-100 cm, 100-300 cm, 300-600 cm, and particles larger than 600 cm in panels b-c are shown in light blue, blue, light green, and green. (d) Cumulative grain size distribution of the on-site sample with size < 100 mm.

批注 [hL8]: We corrected the sequence number of the composite neutron diagram

63% of the particles are concentrated in three zones A1, A2, A3 (**Figs. 8a-b**). The three zones are gentle banks or floodplains. The large stones easily slowed down when the flow depth and the velocity decreased on the edges of the debris flows. The composition of the particles in A1-A3 exhibits similar grain size distribution (**Fig. 8b**). The size of the most numerous particles is between 100 and 300 cm. The stones with the size > 600 cm are the least. The number of particles with 100-300 cm size accounts for 77.4% of the total. Likewise, the particles with sizes of 50-100 cm, 300-600 cm, and >600 cm, accounted for 14.3%, 7.7%, and 0.6% of the total, respectively. If the particle volume is estimated with the equivalent ellipsoid volume, i.e.  $V = (4\pi abc) / 3$  (where  $a$  is major radius,  $b$  is short radius,  $c$  is polar radius and equal to  $b$ ), the two groups of particles with the sizes of 100-300 cm and 300-600 cm have the largest volume.

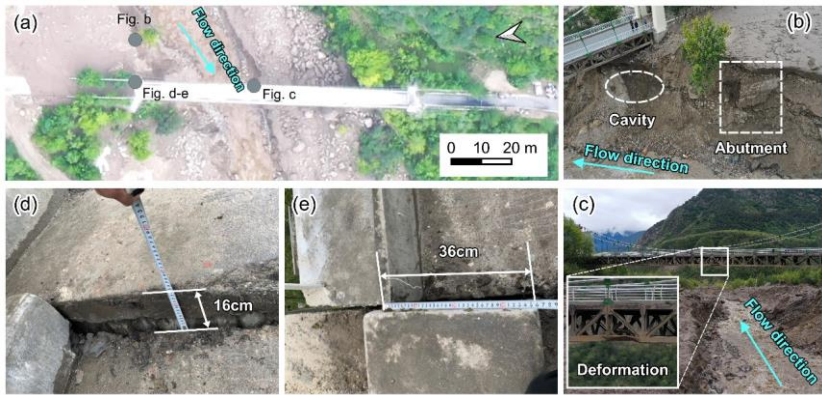
The spatial distribution of these particles in the 45 segments is shown in **Figure 8c**. The same four size ranges are used (50-100 cm, 100-300 cm, 300-600 cm, and > 600 cm). The particles with the first three sizes have three peaks in A1, A2, and A3 (**Fig. 8c**). The first peak is located on the right bank highland of A1. When the debris flows moved to A1, the flow depth was far higher than the channel depth. Many coarse particles were left on the highland. The second peak is located on both channel sides above Zhibai Bridge. When the debris flow enters the bend at a high speed, a large velocity difference will be generated on the concave-convex bank, i.e., the super-elevation effect (Chen et al., 2009). The debris flows produced the super-elevation effect when they moved to A2, a partially curved channel. Then, some coarse particles overflowed the channel and deposited on the A2 banks. The third peak is at the top of the alluvial fan. When the debris flows moved out the ~~mouth-catchment outlet~~ and had no boundary constraint, the other coarse particles gradually deposited from the fan top to the fan edge due to loss of kinetic energy. In the A1 highland, the particle size decreased toward the outer edge of the channel (**Fig. 8-a2**), while the coarse particles in A2 were poorly sorted (**Fig. 8-a3**). In A3, the coarse particles on the surface show the parallel superposition of two depositional units, and the particle size of each depositional unit generally decreases toward the outer edge of the channel (**Fig. 8-a4**). It reflects the gradual accumulation of multiple debris-flow surges (Sohn, 2000; Major, 1998). The two depositional units may correspond to the two successive debris flow surges in ~~Zelunglung-ZLL~~ at 5:00 pm and 6:00 pm.

### 4.2.3 Impact and erosion

Debris flows usually have steep coarse-grained surge fronts (snouts) and inter-surge watery flows (McCoy et al., 2013; Yan et al., 2023). The periglacial debris flows in ~~Zelunglung-ZLL~~ had similar spatial compositions. The granular flows (coarse-grained snouts) at the fronts exerted a powerful impact on obstacles, and the inter-surge watery flows or water-rich tails with relatively low sediment concentration played critical roles in erosion. The ~~Zelunglung-ZLL~~ debris flows had a very high content

375 of coarse particles and wide distribution. The impact of the coarse particles witnessed by the damages of the Zhibai bridge, a  
376 100m long cable bridge with a steel frame (Fig. 9a). The foundation of the bridge was exposed by the strong erosion capacity  
377 of the debris flows (Fig. 9b). The middle steel frame was intensely impacted by run-up boulders and highly deformed (Fig.  
378 9c). The concrete bridge body displaced 16 cm in vertical direction and 36 cm in horizontal direction (Figs. 9d and e). The  
379 velocity of the largest boulder with a size of 9.9 m was  $12.6 \text{ m/s}$ , and the impact force of the largest boulder was estimated  
380 to be  $3.64 \times 10^6 \text{ kN}$ . The velocity of the debris flow at the selected cross section near the Zhibai bridge was  $9.65 \text{ m/s}$ , the peak  
381 value of debris-flow runoff was  $1743.4 \text{ m}^3/\text{s}$  (Fig. 10) (Li et al., 2024).

382  
383 Figure 9: Damages to the Zhibai Bridge caused by debris flows (photos taken on 11 Sep 2020). (a) The overview of Zhibai Bridge  
384 taken by UAV and the locations shown in photographs (b)-(e) taken with handheld cameras are shown in gray circles. (b) The photo  
385 of the damaged bridge foundation. (c) The photo of the damaged steel frame. (d) Photo of on-site measurements of the vertical  
386 displacement of the bridge. (e) Photo of on-site measurements of the horizontal displacement of the bridge.



设置了格式: 字体: (默认) Times New Roman, (中文) Times New Roman



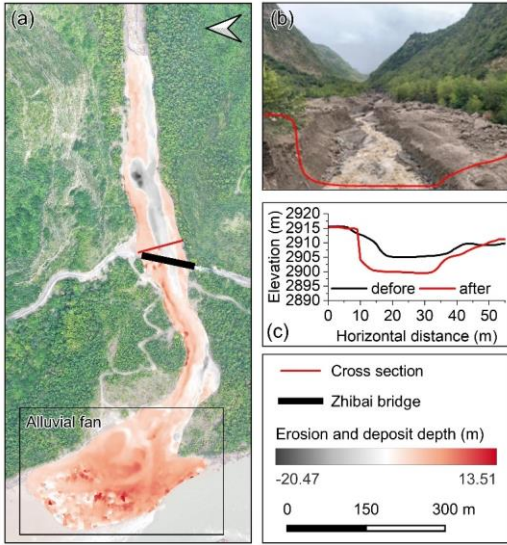


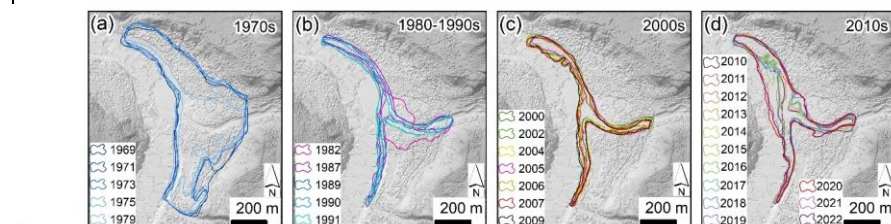
**Figure 10: Geomorphic changes of the channel and alluvial fan after the debris flows of 2020. (a) Erosion and deposit depth caused by the debris flows. The base map is taken by UAV on 10 Sep 2020. (b) Photo of the channel after the debris flows. The red line represents the cross-section next to the Zhibai Bridge (photo taken on 11 Sep 2020). (c) Cross-sections before (black) and after (red) the debris flows.**

A vibrating sieve measured one sample taken from the debris-flow deposits with the size  $< 100$  mm. The concentration of sediment finer than  $0.075$  mm is low, only  $3.8\%$  of the whole sample's mass (**Fig. 8d**).  $D_{50}$  and  $D_{90}$  of the sample are  $8.3$  mm and  $62.9$  mm, respectively, as linearly interpolated from the sieve-measured data. The field evidence shows that the debris flows strongly eroded the downstream channel. Comparing the ~~drone-obtained Digital Surface Model (DSM)s~~ data before and after the ~~9-10-2020~~ event, the maximum erosive depth was up to  $20.47$  m, and the mean erosive depth was  $4.17$  m (**Fig. 10a**). Peng et al. (2022) numerically simulated the final erosion and deposition along the flow path. The maximum erosion depth was  $7.41$  m at the beginning of the downstream channel. We think the simulation underestimates the erosion depth because the final erosion accumulates several erosive watery flows. Lateral erosion happened nearly along the whole downstream channel. The channel width increased from  $17$  m to  $33$  m at  $70$  m upstream of the bridge. The lateral erosion exposed the bridge foundation, and a cavity formed below the pier (**Fig. 9b**). Concave bank erosion widened the channel by  $14$  m downstream. Based on the DoD, we estimated that at least  $12.8 \times 10^4 \text{ m}^3$  ( $\pm 1.85 \times 10^4 \text{ m}^3$ ) of debris was transported out of the catchment (**Fig. 10a**). However, compared with the study of Peng et al. (2022), the true volume may be seriously underestimated because part of the sediment may be submerged by the Yarlung Tsangpo River, which is a bias caused by the difference in data acquisition time and DEM/DSM resolution.

406 **5 Multi-periodic Sedimentation in the confluence**

407 Multi-periodic periglacial debris flows are strongly related to variations in the NVA of the alluvial fan. In practice, the NVA  
408 includes a fixed part of the area inundated by the river and then is larger than the debris-flow depositional or flooded area (Fig.  
409 11). Technically, the NVA caused by the main river cannot be completely excluded from the total area. However, the river  
410 bank line was fixed from the 1980s to the 2010s when no large periglacial debris flows happened (Figs. 11b and c) (Zhang  
411 and Shen, 2011). So, it is reasonably assumed that the variation of the river water level has no significant influence on the  
412 NVA's change, and it represents the volume trend of the sediment transported by the debris flows.

413 From the Keyhole satellite image in 1969, the deposited debris from the 1968 event resided on the confluence and covered a  
414 2.5 km downstream reach of the Yarlung Tsangpo River from the junction (Fig. 3a) (Kääb et al., 2021). During 1969 – 1979,  
415 the area of the accumulated fan kept at about 0.28 km<sup>2</sup>. The 1979-1972 image shows vegetation gradually developed from the  
416 edge of the accumulation fan (Fig. 3-b2). A new channel developed along the 1972 deposition boundary across the middle of  
417 the fan (Fig. 3f3b-2). Since then, the area without vegetation cover has reduced to 0.048 km<sup>2</sup> in 2005 and kept a slight  
418 fluctuation from 1985 to 2005. It indicates that only rainfall-induced small-scale flash floods or debris flows occurred during  
419 1985-2005, which is confirmed by Zhang and Shen (2011). The NVA increased slowly, with a slight variation from 2005-  
420 2019. In 2020, the NVA abruptly increased to 0.112 km<sup>2</sup> due to the ice-rock avalanche that happened on September 10 (Fig.  
421 11). The expansion of NVA in 2020 demonstrates it is the most enormous debris flow event in the Zelunglung-ZLL since 1972.  
422 At the same time, the river channel narrowed down by more than 60 meters compared to before. The multi-periodic  
423 sedimentation in the Zelunglung-ZLL and Zhibai fans leads to rapids in this reach, forming a knickpoint before the river enters  
424 the Yarlung Tsangpo Grand Canyon.



425  
426 **Figure 11: Evolution of the non-vegetated area in the Zelunglung alluvial fan from 1969 to 2022**

427 **6 Discussions**

428 **6.1 The dominant factor for debris flows and sediment yield**

429 Strong ground vibrations caused by earthquakes can intensify cracking within the ice/rock mass, ultimately leading to the  
430 formation of substantial failure surfaces (Kilburn and Voight, 1998). Additional loading by earthquakes and coseismic-ice/rock

设置了格式: 字体颜色: 红色

设置了格式: 字体: 加粗

设置了格式: 上标

431 avalanches could ~~damage destruct~~ the englacial conduit and subglacial drainage system. These changes can cause dynamic  
432 alterations to the glacier's thermal sensitivity, exacerbating its instability (Zhang et al., 2022b). As critical solid material sources,  
433 these highly active ice/rock masses caused by seismic disturbance are prone to avalanches, calving, detachment and  
434 remobilization to form glacial debris flows (Deng et al., 2017; Zhang et al., 2022b). The data of seismic events since 1940 are  
435 collected from the United States Geological Survey (USGS) National Earthquake Center (NEIC)  
436 (<https://earthquake.usgs.gov/earthquakes/search/>) (Fig. 12a). It is observed that the four events in the ~~Zelunglung~~ ZLL in 1950,  
437 1968, 1984, and 2020 were preceded by significant seismic activity. ~~Nearly 30 earthquakes with  $M_w \geq 4.5$  occurred within~~  
438 ~~one year before the 2020 debris flow event (10 September 2019–10 September 2020) whose epicentres are less than 200 km~~  
439 ~~away from the Zelunglung~~. However, not all earthquakes influenced the instability of ~~Zhelunglung's~~ ZLL glaciers and  
440 hillslopes. Keefer (1984) presented an upper bound curve of maximum distance from epicenter to disrupted slide or fall (Fig.  
441 13). Since 1940, only 12 earthquakes within a 420-km radius of ZLL fall below the bound curve, including the 1947 earthquake,  
442 the 1950 Assam earthquake and its aftershocks, the 1985 earthquake, and the 2017 Milin earthquake. ~~If including the inundated~~  
443 ~~area of  $\sim 0.78 \text{ km}^2$  in 1950, the alluvial area disturbed by debris flows or floods decreased until 1990 and then kept at a low~~  
444 ~~value before 2020 (Fig. 12d). If the 1950 debris flow event was directly triggered by the 1950 Assam earthquake, as Zhang~~  
445 ~~(1992) suggested, the earthquake effect becomes negligible 40 years later, as the understability of the glacier materials caused~~  
446 ~~by the earthquake may have improved.~~ Notably, ~~the impact distance of a large earthquake can reach hundreds of kilometers.~~  
447 ~~For example, the co-seismic landslides triggered by the 2015 Gorkha  $M_w$  7.8 earthquake extended to a distance of over 130~~  
448 ~~km from the epicenter (Martha et al., 2017) the epicenter of the 1950 earthquake is about 195 km away from the ZLL basin.~~  
449 ~~The 1950 Assam earthquake, with its epicenter approximately 199 km from the ZLL, had a very high magnitude ( $M_w$  8.6) and~~  
450 ~~occurred in the tectonically active eastern Himalayan syntaxis. Coupled with subsequent high-magnitude aftershocks near the~~  
451 ~~ZLL (Fig. 13), the seismic impact on the ZLL was significantly amplified despite the distance. This seismic event also~~  
452 triggered a prolonged period of debris flow activity, persisting for decades, in Guxianggou, approximately 50 kilometers  
453 northeast of the ZLL Valley (Du and Zhang, 1981). Although 13 earthquakes of  $M_w > 5.1$  occurred in 1968 and 6 earthquakes  
454 of  $M_w \geq 4.5$  occurred in 1984, ~~none of these seismic events fell within the range of influence as defined by the Keefer curve~~  
455 ~~(Fig. 13) the Keefer curve did not detect any of these seismic events.~~ This suggests that these earthquakes did not have a  
456 significant influence on the debris flow events of 1968 and 1984. ~~The 1950 debris-flow event was directly triggered by the~~  
457 ~~1950 Assam earthquake (Zhang, 1992), and the root causes of the 1968, 1972 and 1984 events were the structural damage to~~  
458 ~~the glacier and its exposure to lower altitudes with higher temperatures, both resulting from the 1950 earthquake. If including~~  
459 ~~the inundated area of  $\sim 0.78 \text{ km}^2$  in 1950, the alluvial area disturbed by debris flows or floods decreased by 91% until 1990 and~~  
460 ~~then kept at a low value before 2020 (Fig. 12d). If the 1950 debris flow event was directly triggered by the 1950 Assam~~  
461 ~~earthquake, as Zhang (1992) suggested, This means the earthquake effect becomes negligible 40 years later, as the~~  
462 ~~understability of the glacier materials caused by the earthquake may have improved.~~ While the highest frequency of  
463 earthquakes occurred near the time of the 2020 event, they could be ignored due to their small magnitude ( $M_w < 5.2$ ) and long

设置了格式: 字体颜色: 深红

设置了格式: 字体颜色: 深红

批注 [hL9]: Reviewer #2

One of the problems is that the authors do not present any higher resolution imagery between the 1950 event and 1969 (first image). The conclusions about the influence of the 1950 Assam earthquake on debris flow activity from the glacial area over 40 years are based on weak data (first manuscript version). The increasing influence with time of climatic triggers is not enough taken into consideration. Also the stats-graphs are not clear about that influence.

As such, defenders of the pure climatic influence on high-mountain hazards (see some recent papers about this analysis in the Andes) will continue to believe that those types of hazards are influenced by earthquakes only immediately after the event.

Additionally, I think that without modelling this long-term effect of earthquakes on natural hazards (and see .. site located more than 100! km away from the Assam epicentral region!), especially on such high-mountain hazards, will not be proved especially if no high-quality image material is available for the time before and after the earthquake (as in this case, with the main seismic event in 1950 !). Even for the Wenchuan earthquake, the longterm influence on increased geohazard activity is considered to have finished after 10years (as indicated by the authors as well), even for sites very close to the activated fault.

Concluding: as the authors present a very detailed study, I would still recommend a major revision (and not rejection) - but the discussion should more highlight the extreme uncertainty affecting this 'extreme long-term' effect of a major earthquake in high-mountain areas (which are obviously the most strongly affected by climatic variations), especially as the zone is located so far from the epicentral area, and also of the fault (if I see well).

● Author's response:

Thank you very much for your insightful comments.

Unfortunately, we were unable to obtain high-resolution remote sensing imagery for the period between the 1950 event and 1969, which indeed would provide the most direct evidence. However, the 1950, 1968, and 1984 events are well-documented in the literature (Zhang and Shen, 2011; Zhang, 1985, 1992). The 1950 event occurred immediately following the Assam earthquake and is considered to be directly associated with the seismic activity.

Notably, the earthquake triggered simultaneous debris flows in as many as 13 gullies in the Yarlung Tsangpo Grand Canyon area (Liu, 1984). During the 1950 event, the terminus of the ZLL trunk glacier advanced from 3650 m a.s.l to the Yarlung Tsangpo at 2810 m a.s.l, forming a glacial dam in the Yarlung Tsangpo River. During the 1968 event, the ZLL Glacier again formed a dam over 50 m high in the Yarlung Tsangpo River, while the 1972 event was similarly caused by the local collapse of the glacier terminus (...)

设置了格式: 字体: 加粗

设置了格式: 字体: 加粗

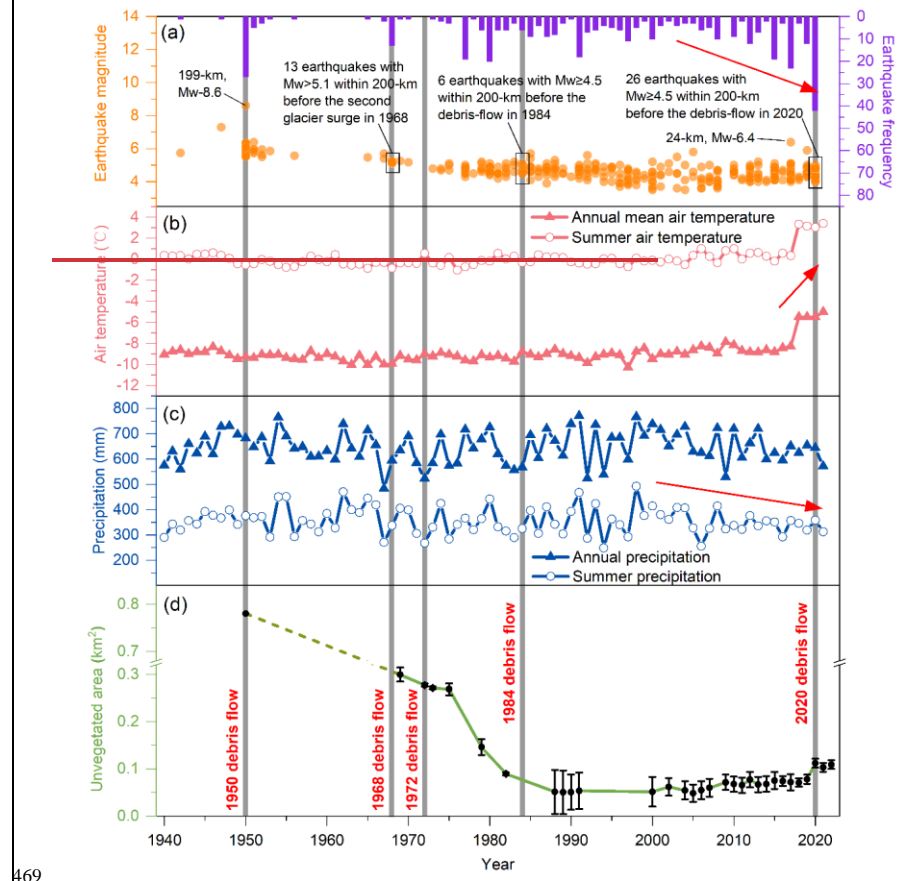
批注 [hL10]: L414: What do you mean by “the Keefer curve did not detect any of these seismic events”? A curve cannot detect anything.

● Author's response:

Thank you for pointing out this unclear statement. The phrase "the Keefer curve did not detect any of these seismic events" is indeed poorly worded and could be misleading. The statement "the Keefer curve did not detect any of these seismic events" is a metaphorical (...)

设置了格式: 字体: 加粗

464 distance (>30km) (Fig 13). This is because even The the 2017 Mw 6.4 Milin earthquake, of which the with an epicenter is 24  
465 km from the ZelunglungZLL, had a very limited impact area (310 km<sup>2</sup>, ~10 km impact radius) (Hu et al., 2019), probably has  
466 limited influence on its glacial activity because- and there is were no report or sign on of such glacier-related hazards in the  
467 ZelunglungZLL. However, there are direct proofs that the Milin earthquake caused the 2018 glacier surges and extra large-  
468 scale debris flows in the Sedongpu (Hu et al., 2019; Zhang et al., 2022b), 25 km downstream of the ZelunglungZLL.



设置了格式: 字体: 加粗

批注 [hL11]: Reviewer #2

One of the problems is that the authors do not present any higher resolution imagery between the 1950 event and 1969 (first image). The conclusions about the influence of the 1950 Assam earthquake on debris flow activity from the glacial area over 40 years are based on weak data (first manuscript version). The increasing influence with time of climatic triggers is not enough taken into consideration. Also the stats-graphs are not clear about that influence. As such, defenders of the pure climatic influence on high-mountain hazards (see some recent papers about this analysis in the Andes) will continue to believe that those types of hazards are influenced by earthquakes only immediately after the event. Additionally, I think that without modelling this long-term effect of earthquakes on natural hazards (and see .. site located more than 100! km away from the Assam epicentral region!), especially on such high-mountain hazards, will not be proved especially if no high-quality image material is available for the time before and after the earthquake (as in this case, with the main seismic event in 1950!). Even for the Wenchuan earthquake, the longterm influence on increased geohazard activity is considered to have finished after 10years (as indicated by the authors as well), even for sites very close to the activated fault. Concluding: as the authors present a very detailed study, I would still recommend a major revision (and not rejection) - but the discussion should more highlight the extreme uncertainty affecting this 'extreme long-term' effect of a major earthquake in high-mountain areas (which are obviously the most strongly affected by climatic variations), especially as the zone is located so far from the epicentral area, and also of the fault (if I see well).

● Author's response:

Thank you very much for your insightful comments. Unfortunately, we were unable to obtain high-resolution remote sensing imagery for the period between the 1950 event and 1969, which indeed would provide the most direct evidence. However, the 1950, 1968, and 1984 events are well-documented in the literature (Zhang and Shen, 2011; Zhang, 1985, 1992). The 1950 event occurred immediately following the Assam earthquake and is considered to be directly associated with the seismic activity. Notably, the earthquake triggered simultaneous debris flows in as many as 13 gullies in the Yarlung Tsangpo Grand Canyon area (Liu, 1984). During the 1950 event, the terminus of the ZLL trunk glacier advanced from 3650 m a.s.l to the Yarlung Tsangpo at 2810 m a.s.l, forming a glacial dam in the Yarlung Tsangpo River. During the 1968 event, the ZLL Glacier again formed a dam over 50 m high in the Yarlung Tsangpo River, while the 1972 event was similarly caused by the local collapse of the glacier terminus (Fig. S7-b3 and c3). The images from 1979 also show significant glacier fragmentation and differential ablation (Fig. S7-e3). Compared to 1979, glacier ablation intensified in 1982, exposing lateral moraines (Fig. S7-e2 and S7-f3), and the lowest section of the glacier developed numerous crevasses (Fig. S7-f4 and S7-f5). These fractured ice bodies and moraine materials, under the impact of the 1984 ice avalanche at 3700 m observed by the First Qinghai-Tibet Scientific Expedition (Zhang, 1992), contributed to the formation of the 1984 large-scale debris flow. By 1989, three of the glacier segments had melted, detached from the main glacier, and were buried under thick moraine deposits. These events clearly indicate that the frequent ruptures, collapses, and differential melting of the ZLL Glacier were associated with disturbances caused by the 1950 earthquake. While rising temperatures likely contributed to the melting and instability of ...

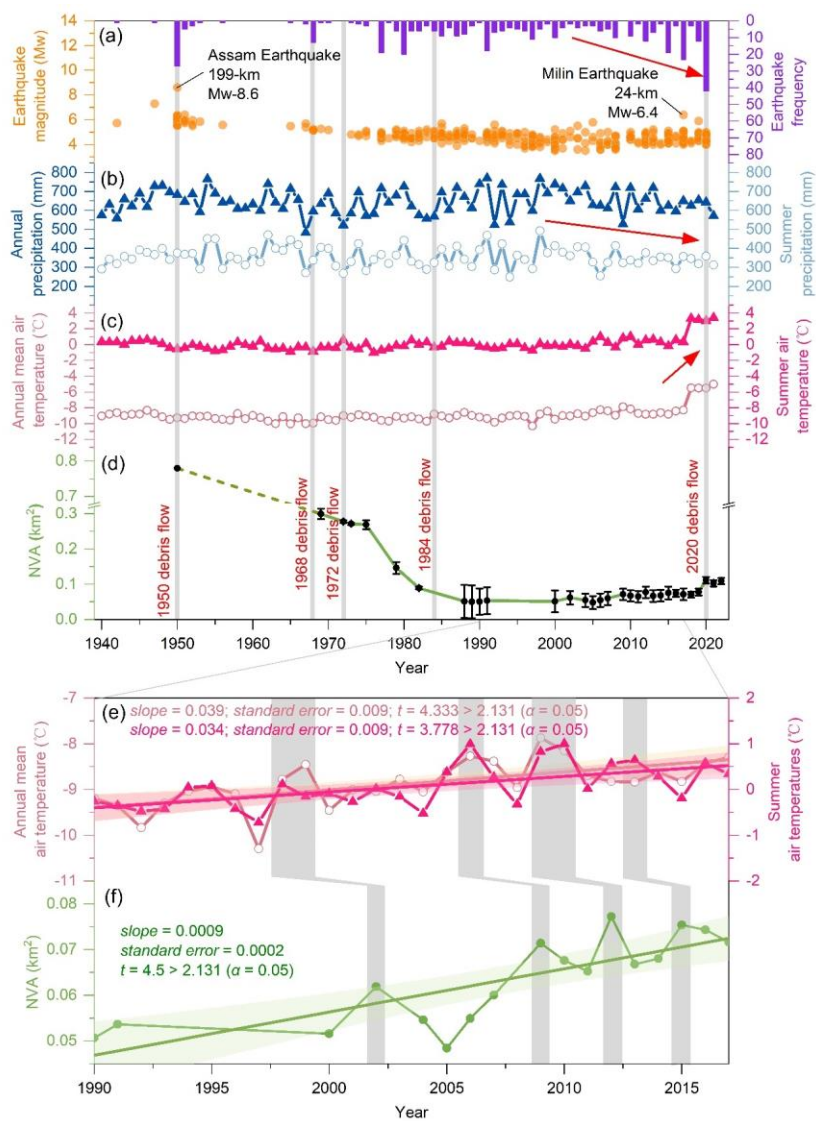




Figure 12: (a) Seismic events within a 200 km distance to the Zelunglung from 1940 to the present. (b) Changes in the annual mean and summer air temperatures in the Zelunglung from 1940 to the present. (c) Changes in the annual and summer precipitation in the Zelunglung from 1940 to the present. (d) Changes in the non-vegetated area of the Zelunglung alluvial fan from 1969 to the present (although the deposition of the 1950 event did not happen at the Zelunglung's outlet like the later events, we plot the NVA of the 1950 event as the starting point), (e) Changes in the annual and summer precipitation in the Zelunglung from 1990 to 2017, (f) Changes in the non-vegetated area of the Zelunglung alluvial fan from 1990 to 2017.

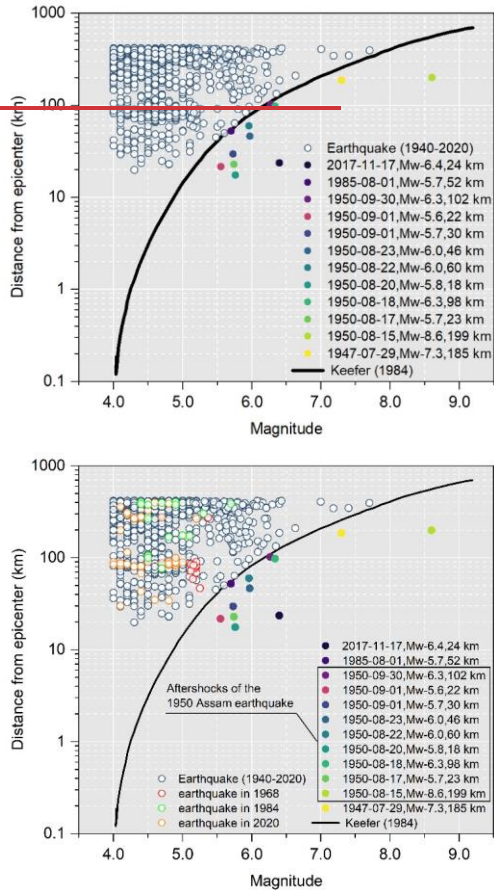


Figure 13: Distance from epicenters of the collected seismic events to the Zelunglung vs. the seismic magnitude (the black solid curve refers to Keefe (1984)).

批注 [hL12]: We included magnified charts depicting the temperature and NVA data spanning from 1990 to 2017.

设置了格式: 字体: (中文) + 中文正文 (宋体)

设置了格式: 字体: (中文) + 中文正文 (宋体)

批注 [hL13]: In the figure, we highlight the earthquakes preceding the 1968, 1984, and 2020 events.

Furthermore, we extracted the gridded mean values of annual mean air temperature, summer air temperature, annual precipitation, and summer precipitation within the *Zelunglung-ZLL* catchment during 1940 - 2021 from a dataset for China (1901-2021) (Peng, 2019) and 1-km monthly precipitation dataset for China (1901-2021) (Peng, 2020), respectively (Fig. 12b and c). These data were validated using 496 independent meteorological observation points (Peng et al., 2019). From 1940 to 2017, the annual mean and summer air temperatures at the *Zelunglung-ZLL* kept relatively stable. However, in 2018, there was a sudden and significant increase in the annual mean and summer air temperatures, with an amplitude exceeding 2.5 °C. Since then, the temperatures have maintained at a high level. There has been no significant change in annual and summer precipitation since 1940, but a slight decreasing trend has been observed since 2000. The rates of atmospheric warming in the Tibetan and Himalayan regions are far higher than the general global warming rate since 1960, which accelerates the rates of most glaciers shrinking and ice mass loss across the regions (Shugar et al., 2021; Zhang et al., 2020). Undoubtedly, the on-going warming increases the frequency of such glacier-related slope failures. Recent studies have shown that the on-going climate warming increases the frequency of such glacier-related slope failures. For instance, The number of rockfalls per decade show a similar growing trend with mean annual air temperature in Chamonix, Mont Blanc massif, France since 1934 (Deline et al., 2015). The frequency of non-seismic rock avalanches in the glaciated Saint Elias Mountains of Alaska was associated with above-average temperatures and is expected to continue increasing with ongoing climate warming (Bessette-Kirton and Coe, 2020). Shugar et al. (2021) suggested that the 2021 Chamoli catastrophic ice-rock avalanche and subsequent mass flow resulted from a complex response of the geologic and topographic settings to regional climate change. Figure 12f highlights four distinct NVA peaks, which likely correspond to small mountain torrent or debris-flows, as suggested by Zhang and Shen (2011). These NVA peaks exhibit a lag of 2–4 years relative to annual mean or summer air temperature peaks (Figure 12e and 12f). Similarly, the sharp increase in NVA caused by the 2020 debris flow event occurred two years after the 2018 warming anomaly (Fig. 12b and 12d). This lag phenomenon has also been observed in other comparable regions (Stoffel et al., 2024). Even though there is no direct observation data of surface temperature in the *Zelunglung-ZLL* highland, the three years of intense warming may change the thermal and hydrological conditions of the *Zelunglung-ZLL* glaciers, such as the thermal regime at the rock-ice contact surface, melting rate of the surface ice and snow, englacial drainage system, fostering the instability of ice-rock blocks on the top. Previous intense seismic shaking could widen rock fractures and reduce the ice-rock strength. It is no doubt that the 2020 *Zelunglung-ZLL* event is the product of the interplay among geological movement, steep topography, and climate warming. However, based on the fact that the lag relationship between the fluctuation peaks of NVAs and temperature fluctuations from 1990 to 2020, the trend of the 1990–2020 NVAs shows a good agreement with that of the air temperature in the same period, it is likely that the 2020 event was triggered driven by the recent local warming rather than by geological events such as the mass flow event in 1950.

It is evident that either earthquakes or climate change may increase the occurrence of periglacial debris flows and their sediment yield in southeastern Tibet (Du and Zhang, 1981; Deng et al., 2017; Wang et al., 2023). In the case of *Zelunglung-ZLL*, the NVA closely related to the debris flows decreased until 1990 and slightly fluctuated increased around a low level until 2020.

批注 [hL14]: 说一下前几次峰值小于 2018, 说明更有可能引发大规模泥石流

批注 [hL15]: L440: "show a similar growing trend". Similar to what?

Author's response:

There is an important increase in the frequency of rock falls and a strong correlation between the warmest periods and the occurrence of 58 rock falls in the Mont Blanc massif. As shown in Figure S6, the number of rockfalls per decade show a similar growing trend with mean annual air temperature in Chamonix, Mont Blanc massif, France since 1934 (Deline et al., 2015).



Figure S6: Mean annual air temperature in Chamonix (1,040 masl) since 1934 and number of rock falls per decade in the West face of the Drus and on the North side of the Aiguilles de Chamonix, Mont Blanc massif, France. Dashed lines: linear regressions.

设置了格式: 字体颜色: 深红

设置了格式: 字体颜色: 深红

批注 [hL16]: (iii) There are also suggestions in the manuscript in places that the climate change increases the frequency of debris flow events. (e.g. L439: "Undoubtedly, the on-going warming increases the frequency of such glacier-related slope failures"). I am not convinced the data in this work speak to the presence or absence of such a link, and the link between climate change and glacier-related natural hazards can be complex. For example, the frequency of GLOFs does not necessarily just simply increase with climate warming (Veh et al., 2019; Veh et al., 2023)

● Author's response:

Thank you very much for your insightful comments. It is important to clarify that the statement in L439 is not derived directly from the data in this study. We agree that the wording in its current form is overly absolute. A more appropriate revision would be: "Recent studies have shown that the on-going climate warming increases the frequency of such glacier-related slope failures." Following this statement, we have cited case studies from similar regions globally to support the argument that the 2020 event in the ZLL basin was very likely driven by warming.

● Author's changes in manuscript:

To clarify, we revised the sentence as follows:

Recent studies have shown that the on-going climate warming increases the frequency of such glacier-related slope failures.

设置了格式: 字体颜色: 深红

设置了格式: 字体颜色: 深红

设置了格式: 字体颜色: 深红

设置了格式: 字体: 加粗

设置了格式: 字体颜色: 深红

批注 [hL17]: L448: "the trend of the 1990-2020 NVAs shows a good agreement with that of the air temperature in the same period".

● Author's response:



514 That means the effects of the 1950 earthquake were decaying; ~~meanwhile, the local air temperature and precipitation had no~~  
515 ~~significant variation until 2018~~. The response of hillslopes or glaciers to earthquakes is immediate. Had the 2017 Milin  
516 earthquake strongly impacted the glaciers in the Zelunglung-ZLL, ice-rock failures would have happened a few months later,  
517 like in the Sedongpu catchment. By contrast, the response of glaciers to warming will take longer. Meanwhile, approximately  
518 one month prior to the 2020 debris flow event, the maximum temperature recorded was 27°C, ~~with a~~ accompanied by a peak  
519 precipitation of ~~only merely~~ 17.5mm. Notably, on the day the 2020 debris flow occurred, the steel bridge deck ~~remained was~~  
520 dry, ~~indicating suggesting~~ that the precipitation was very light (Peng et al., 2022). On the other hand, the magnitude of the  
521 warming-driven debris flows is smaller than that of the earthquake-driven. We believe the abrupt 2.5 °C warming in 2018-  
522 2020 is dominant in initiating the 2020 ice-rock avalanche.

523 **6.2 The future risk**

524 Zhang et al. (2022a) predicted that cryosphere degradation driving the increasing sediment yield in cold regions is likely to  
525 shift from a temperature-dependent regime toward a rainfall-dependent one in the next century. But in tectonically active high-  
526 altitude areas, the temperature-dependent and the earthquake-dependent regimes will alternate in the future.

527 The period of the Zelunglung-ZLL glacier surges is getting shorter. Zhang (1985) supposed that the surging cycle of the  
528 Zelunglung-ZLL glacier was about 20 years. According to the latest research by Guillet et al. (2022), the Zelunglung-ZLL  
529 glacier showed signs of surge in 2004, 2005, and 2006. Moreover, there are more obvious signs of a surge in 2016-2015 (**Fig.**  
530 **14**). The interval between the last two surges is ten years, which shows that the surging cycle of the Zelunglung-ZLL glacier  
531 may be decreasing, and the next large-scale surge may happen in the next ten years. Furthermore, changes in the speed of  
532 glacier movement can strongly impact channel side moraines or terminal moraines and lead to slope failures (Richardson and  
533 Reynolds, 2000). The potential ice collapse area in the formation area of the Zelunglung-ZLL catchment is 2.4 km<sup>2</sup>, the rock  
534 collapse area reaches 0.96 km<sup>2</sup>, and the loose moraine accumulation reaches 5.2 km<sup>2</sup> (Li et al., 2021; Liu et al., 2022). However,  
535 the ~~"9.10"~~ 2020 debris flow was caused by a relatively small area of ice-rock collapses in the formation area, which is only the  
536 tip of the iceberg compared to the overall high-risk provenances in the formation area of the Zelunglung-ZLL catchment. That  
537 means if intense earthquakes or extreme warming events happen not far away from the catchment, the risk of slope failures or  
538 glacier detachment on the steep slopes and ridges is high and huge amounts of sediment will be transported into the river by  
539 large-scale debris flows.

批注 [hL18]: L459: Unclear which of the debris flows "the debris flow" corresponds to (presumably the 2020 one, but it's unclear from this paragraph).

● Author's response:

Thank you for your suggestion. Yes, the term "the debris flow" in this paragraph refers to the debris flow that occurred in 2020. We have revised the text to replace "the debris flow" with "the 2020 debris flow" for clarity.

● Author's changes in manuscript:

We have revised the text to replace "the debris flow" with "the 2020 debris flow".

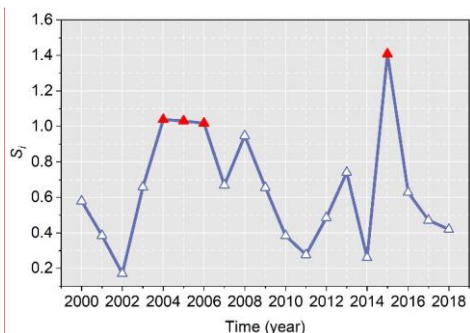
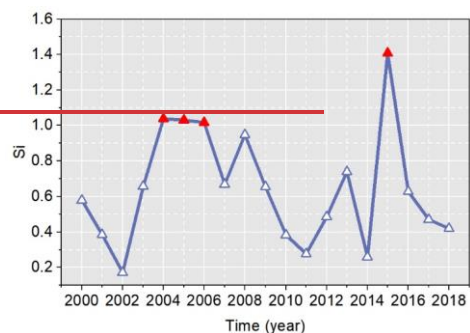


**Figure 14: Surge-index ( $S_i$ ) of Zelunglung Glacier from 2000 to 2018.  $S_i$  is a quantitative index of the surge magnitude, calculated by the formula  $S_i = \frac{IPR_i}{k \cdot V_0}$ , where  $IPR_i$  is the inter-percentile range for year  $i$ ,  $k$  is a threshold for surge identification, and  $V_0$  is the error-weighted mean velocity for the study year. The years with  $S_i > 1$  are marked with red triangles. (Data source: <https://doi.org/10.5281/zenodo.5524861> (Guillet et al., 2022)).**

### 6.3 Effects on river geomorphology

The moraine and old deposits on both channel sides provided numerous boulders for debris flows. The number of coarse particles transported by the Zelunglung-ZLL periglacial debris flows is very high, and there is no obvious particle sorting along the flow path. Most of the boulders are gneiss with high hardness, and the wearing and disintegration effects are not significant during the movement along the channel. Coarse particles are deposited on the platform at the bend and the top of the alluvial fan, where the channel suddenly widens. Such phenomenon demonstrates that the movement, deposition, and particle size distribution of the debris flow are not only related to the type of debris flow (Bardou et al., 2003) but also to topographic conditions (Ghilardi et al., 2001; Zhou et al., 2019).

批注 [hL19]: Fixed the vertical axis title by changing  $S_i$  to  $S_i$

设置了格式: 字体: (中文) + 中文正文 (宋体)

554 The deposition of the “9.10”2020 debris flow narrowed the Yarlung Tsangpo River at the ~~mouth-outlet~~ of the ~~ZelunglungZLL~~,  
555 and the river bed was significantly elevated. The river flow hardly transports the boulders on the alluvial fan. The peak  
556 discharge of the largest flood in the Yarlung Tsangpo recorded by the hydrologic station at Nuxia, 40 km upstream of the  
557 ~~ZelunglungZLL~~, is 16800 m<sup>3</sup>/s. The maximum size of the particles in such a flood is about 150 cm. The floods capable of  
558 moving the coarsest boulders (> 600 cm) deposited on the ~~Zelunglung-ZLL~~ fan should be on the order of 10<sup>6</sup> m<sup>3</sup>/s of peak  
559 discharge (Lang et al., 2013). Such high-magnitude floods in the Yarlung Tsangpo were caused by catastrophic breaching of  
560 landslide or glacial dams, e.g., several Quaternary megafloods in the middle and downstream of Yarlung Tsangpo (Hu et al.,  
561 2018; Liu et al., 2015; Yang et al., 2022), rather than caused by monsoonal runoffs. Modern outburst floods higher than 10<sup>5</sup>  
562 m<sup>3</sup>/s only happened on the Yigong River, a downstream tributary of the Yarlung Tsangpo Gorge (Hu et al., 2021). Therefore,  
563 the time to evacuate the coarse sediments on the alluvial fan is two orders of magnitude of the recurrence period of periglacial  
564 debris flows. The long-lived protruding fan forms a knickpoint at the confluence. The repeated glacial and landslide dams in  
565 the margin of the Tibetan Plateau play significant roles in reducing the river incision into the plateau interior together with the  
566 moraine dams in the glaciation ages (Hu et al., 2021).

## 567 7 Conclusions

568 High-magnitude sediment evacuation by periglacial debris flows is a crucial surface process that links sediment yield from  
569 high-altitude slopes to river sediment transportation. The ongoing glacier degradation in the Himalayan mountains in response  
570 to recent earthquakes and climate change increases the frequency of the debris flows and their sediment volume. The  
571 ~~Zelunglung-ZLL~~ catchment in the tectonically active eastern Himalayan syntaxis with a high uplift rate has recorded five  
572 periglacial debris flow events since 1950. These events delivered huge volumes of sediment into the Yarlung Tsangpo River.  
573 We examine the history of the five events and their sediment characteristics, especially the ice-rock-avalanche-triggered event  
574 in 2020, through field investigations and remote sensing interpretations. Some findings are concluded as follows:

- 575 a) The periglacial debris flows have great capacities to erode channels, transport sediment, and impact obstacles. The  
576 maximum values of the erosion depth, the erosion width, and the impact force near the ~~Zelunglung's-ZLL~~ outlet are about  
577 20 m, 14 m, and 3.64×10<sup>6</sup> kN, respectively, in the 2020 event. The debris flows transported a high concentration of coarse  
578 grains with the size > 50 cm. The 100-300 cm grains account for 77.4% of the coarse grains.
- 579 b) Most of the angular rocks moved by the 2020 avalanche were not delivered downward further. The boulders transported  
580 by subsequent debris flows probably originated from the middle of the downstream reaches. The grain size segregation  
581 was not observed between the middle reach and the alluvial channel.
- 582 c) The ~~non-vegetated-area~~NVA of the ~~Zelunglung's-ZLL~~ fan reduced from 0.78 km<sup>2</sup> in 1950 to 0.067 km<sup>2</sup> in 1990, and kept  
583 at a stable low value until 2020, indicating the influence of the 1950 earthquake on the debris-flow sediment transportation  
584 could last 40 years. Compared with the 1999 Chi-chi earthquake and the 2008 Wenchuan earthquake in non-glaciated  
585 areas, the influence period of the 1950 earthquake is much longer.

d) The seismic and local meteorological data show that the recent warming events drove the 2020 debris-flow event during 2018-2020. The surging cycle of Zelunglung's-ZLL glaciers is getting short due to climate change. The correspondence between the recent increases in the local air temperature and the NVA implies that the debris flow occurrences in ZLL transfer from the tectonic-driven to the climatic-driven, with debris flows exhibiting a lagged response of 2-4 years to rising temperatures.

*Acknowledgments.* This research was funded by the Second Tibetan Plateau Scientific Expedition and Research Program (2019QZKK0902) and the National Natural Science Foundation of China (91747207, 41790434). MRG acknowledges the 'ANSO Scholarship for Young Talents' for his postgraduate study.

*Data availability.* All raw data can be provided by the corresponding authors upon request.

*Author contributions.* KHH conceptualized the study, interpreted the images, wrote and edited the manuscript. HL analyzed the data and wrote the manuscript draft. KHH, HL, SL, LW, XPZ, and BZ performed the field surveys. HL and MRG collected satellite and background data. LMZ provided constructive suggestions. All authors contributed to the preparation and editing of the paper.

*Competing interests.* The authors declare that they have no conflict of interests.

## References

- Bajracharya, S. R. and Mool, P.: Glaciers, glacial lakes and glacial lake outburst floods in the Mount Everest region, Nepal, ANN GLACIOL, 50, 81–86, <https://doi.org/10.3189/172756410790595895>, 2009.
- Bardou, E., Ancely, C., Bonnard, C., and Vulliet, L.: Classification of debris-flow deposits for hazard assessment in alpine areas, in: Debris-Flow Hazards Mitigation: Mechanics, Prediction, and Assessment, The Third International Conference on Debris-Flow Hazards Mitigation : Mechanics, Prediction, and Assessment, Davos, Switzerland, 10-12 September 2003, 799–808, ISBN 90-77017-78-X, 2003.
- Bessette-Kirton, E. K. and Coe, J. A.: A 36-Year Record of Rock Avalanches in the Saint Elias Mountains of Alaska, With Implications for Future Hazards, FRONT EARTH SC-SWITZ, 8, <https://doi.org/10.3389/feart.2020.00293>, 2020.
- Chen, D., Xu, B., Yao, T., Guo, Z., Cui, P., Chen, F., Zhang, R., Zhang, X., Zhang, Y., Fan, J., Hou, Z., and Zhang, T.: Assessment of past, present and future environmental changes on the Tibetan Plateau, Chinese Science Bulletin, 60, 3025–3035, <https://doi.org/10.1360/n972014-01370>, 2015.

Chen N., Yang C., Li Z., and He J.: Research on the Relationship between the Calculation of Debris flow Velocity and Its Super Elevation in Bend, *Advanced Engineering Sciences*, 41, 165–171, [https://doi.org/1009-3087\(2009\)03-0165-07](https://doi.org/1009-3087(2009)03-0165-07), 2009.

Costa, J. E.: Paleohydraulic reconstruction of flash-flood peaks from boulder deposits in the Colorado Front Range, *GEOL SOC AM BULL*, 94, 986, [https://doi.org/10.1130/0016-7606\(1983\)94<986:PROFPF>2.0.CO;2](https://doi.org/10.1130/0016-7606(1983)94<986:PROFPF>2.0.CO;2), 1983.

Cui, P., Zhou, G. G. D., Zhu, X. H., and Zhang, J. Q.: Scale amplification of natural debris flows caused by cascading landslide dam failures, *GEOMORPHOLOGY*, 182, 173–189, <https://doi.org/10.1016/j.geomorph.2012.11.009>, 2013.

Cui, Y., Hu, J., Xu, C., Miao, H., and Zheng, J.: Landslides triggered by the 1970 Ms 7.7 Tonghai earthquake in Yunnan, China: an inventory, distribution characteristics, and tectonic significance, *J MT SCI-ENGL*, 19, 1633–1649, <https://doi.org/10.1007/s11629-022-7321-x>, 2022.

Dadson, S. J., Hovius, N., Chen, H., Dade, W. B., Lin, J.-C., Hsu, M.-L., Lin, C.-W., Horng, M.-J., Chen, T.-C., Milliman, J., and Stark, C. P.: Earthquake-triggered increase in sediment delivery from an active mountain belt, *GEOLOGY*, 32, 733, <https://doi.org/10.1130/G20639.1>, 2004.

Dai, L., Scaringi, G., Fan, X., Yunus, A. P., Liu-Zeng, J., Xu, Q., and Huang, R.: Coseismic Debris Remains in the Orogen Despite a Decade of Enhanced Landsliding, *GEOPHYS RES LETT*, 48, <https://doi.org/10.1029/2021GL095850>, 2021.

Deline, P., Gruber, S., Delaloye, R., Fischer, L., Geertsema, M., Giardino, M., Hasler, A., Kirkbride, M., Krautblatter, M., Magnin, F., McColl, S., Ravello, L., and Schoeneich, P.: Ice Loss and Slope Stability in High-Mountain Regions, in: *Snow and Ice-Related Hazards, Risks, and Disasters*, edited by: Shroder, J. F., Haeberli, W., and Whiteman, C., Academic Press, Boston, USA, 521–561, <https://doi.org/10.1016/B978-0-12-394849-6.01001-5>, 2015.

Deng, M., Chen, N., and Liu, M.: Meteorological factors driving glacial till variation and the associated periglacial debris flows in Tianmo Valley, south-eastern Tibetan Plateau, *Nat. Hazards Earth Syst. Sci.*, 17, 345–356, <https://doi.org/10.5194/nhess-17-345-2017>, 2017.

Ding, L., Zhong, D., Yin, A., Kapp, P., and Harrison, T. M.: Cenozoic structural and metamorphic evolution of the eastern Himalayan syntaxis (Namche Barwa), *EARTH PLANET SC LETT*, 192, 423–438, [https://doi.org/10.1016/S0012-821X\(01\)00463-0](https://doi.org/10.1016/S0012-821X(01)00463-0), 2001.

Du R. and Zhang S.: CHARACTERISTICS OF GLACIAL MUD-FLOWS IN SOUTH-EASTERN QINGHAI-XIZANG PLATEAU, *Journal of Glaciology and Geocryology*, 10–16, 81–82, 1981.

Evans, S. G. and Clague, J. J.: Recent climatic change and catastrophic geomorphic processes in mountain environments, in: *Geomorphology and Natural Hazards*, edited by: Morisawa, M., Elsevier, Amsterdam, The Netherlands, 107–128, <https://doi.org/10.1016/B978-0-444-82012-9.50012-8>, 1994.

Ghilardi, P., Natale, L., and Savi, F.: Modeling debris flow propagation and deposition, *Physics and Chemistry of the Earth, Part C: Solar, Terrestrial & Planetary Science*, 26, 651–656, [https://doi.org/10.1016/S1464-1917\(01\)00063-0](https://doi.org/10.1016/S1464-1917(01)00063-0), 2001.

Guillet, G., King, O., Lv, M., Ghuffar, S., Benn, D., Quincey, D., and Bolch, T.: A regionally resolved inventory of High Mountain Asia surge-type glaciers, derived from a multi-factor remote sensing approach, *The Cryosphere*, 16, 603–623, <https://doi.org/10.5194/tc-16-603-2022>, 2022.

Haeberli, W. and Whiteman, C. A. (Eds.): *Snow and ice-related hazards, risks, and disasters*, Elsevier, Amsterdam, The Netherlands, 755pp., <https://doi.org/10.1016/C2018-0-00970-6>, 2021.

Han L. and Feng Q.: Analysis of Development Characteristics and Genetic Mechanisms of Glacier Debris Flows in the Zelongnong, MT. Namjagbarwa, Inner Mongolia Science Technology & Economy, 58–59, <https://doi.org/CNKI:SUN:NMKJ.0.2018-04-029>, 2018.

Hu, G., Yi, C.-L., Liu, J.-H., Wang, P., Zhang, J.-F., Li, S.-H., Li, D., Huang, J., Wang, H., Zhang, A., Shi, L., and Shui, X.: Glacial advances and stability of the moraine dam on Mount Namcha Barwa since the Last Glacial Maximum, eastern Himalayan syntaxis, *Geomorphology*, 365, 107246, <https://doi.org/10.1016/j.geomorph.2020.107246>, 2020.

Hu, H.-P., Feng, J.-L., and Chen, F.: Sedimentary records of a palaeo-lake in the middle Yarlung Tsangpo: Implications for terrace genesis and outburst flooding, *QUATERNARY SCI REV*, 192, 135–148, <https://doi.org/10.1016/j.quascirev.2018.05.037>, 2018.

Hu, K., Zhang, X., You, Y., Hu, X., Liu, W., and Li, Y.: Landslides and dammed lakes triggered by the 2017 Ms6.9 Milin earthquake in the Tsangpo gorge, *Landslides*, 16, 993–1001, <https://doi.org/10.1007/s10346-019-01168-w>, 2019.

Hu, K., Wu, C., Wei, L., Zhang, X., Zhang, Q., Liu, W., and Yanites, B. J.: Geomorphic effects of recurrent outburst superfloods in the Yigong River on the southeastern margin of Tibet, *SCI REP-UK*, 11, 15577, <https://doi.org/10.1038/s41598-021-95194-1>, 2021.

Huang, S., Chen, Y., Burr, G. S., Jaiswal, M. K., Lin, Y. N., Yin, G., Liu, J., Zhao, S., and Cao, Z.: Late Pleistocene sedimentary history of multiple glacially dammed lake episodes along the Yarlung-Tsangpo river, southeast Tibet, *QUATERNARY RES*, 82, 430–440, <https://doi.org/10.1016/j.yqres.2014.06.001>, 2014.

Huggel, C., Haeberli, W., Kääb, A., Bieri, D., and Richardson, S.: An assessment procedure for glacial hazards in the Swiss Alps, *CAN GEOTECH J*, 41, 1068–1083, <https://doi.org/10.1139/t04-053>, 2004.

Iribarren Anaconda, P., Mackintosh, A., and Norton, K. P.: Hazardous processes and events from glacier and permafrost areas: lessons from the Chilean and Argentinean Andes, *EARTH SURF PROC LAND*, 40, 2–21, <https://doi.org/10.1002/esp.3524>, 2015.

Jia, H., Chen, F., and Pan, D.: Disaster Chain Analysis of Avalanche and Landslide and the River Blocking Dam of the Yarlung Zangbo River in Milin County of Tibet on 17 and 29 October 2018, *IJERPH*, 16, 4707, <https://doi.org/10.3390/ijerph16234707>, 2019.

Kääb, A. and Girod, L.: Brief communication: Rapid  $\sim 335 \times 10^6 \text{ m}^3$  bed erosion after detachment of the Sedongpu Glacier (Tibet), *CRYOSPHERE*, 17, 2533–2541, <https://doi.org/10.5194/tc-17-2533-2023>, 2023.

680 Kääb, A., Jacquemart, M., Gilbert, A., Leinss, S., Girod, L., Huggel, C., Falaschi, D., Ugalde, F., Petrakov, D., Chernomorets,  
 681 S., Dokukin, M., Paul, F., Gascoin, S., Berthier, E., and Kargel, J. S.: Sudden large-volume detachments of low-angle mountain  
 682 glaciers – more frequent than thought?, *The Cryosphere*, 15, 1751–1785, <https://doi.org/10.5194/tc-15-1751-2021>, 2021.  
 683 Kargel, J. S., Leonard, G. J., Shugar, D. H., Haritashya, U. K., Bevington, A., Fielding, E. J., Fujita, K., Geertsema, M., Miles,  
 684 E. S., Steiner, J., Anderson, E., Bajracharya, S., Bawden, G. W., Breashears, D. F., Byers, A., Collins, B., Dhital, M. R.,  
 685 Donnellan, A., Evans, T. L., Geai, M. L., Glasscoe, M. T., Green, D., Gurung, D. R., Heijenk, R., Hilborn, A., Hudnut, K.,  
 686 Huyck, C., Immerzeel, W. W., Liming, J., Jibson, R., Kääb, A., Khanal, N. R., Kirschbaum, D., Kraaijenbrink, P. D. A.,  
 687 Lamsal, D., Shiyin, L., Mingyang, L., McKinney, D., Nahirnack, N. K., Zhuotong, N., Ojha, S., Olsenholler, J., Painter, T. H.,  
 688 Pleasants, M., Pratima, K. C., Yuan, Q. I., Raup, B. H., Regmi, D., Rounce, D. R., Sakai, A., Donghui, S., Shea, J. M., Shrestha,  
 689 A. B., Shukla, A., Stumm, D., van der Kooij, M., Voss, K., Xin, W., Weihs, B., Wolfe, D., Lizong, W., Xiaojun, Y., Yoder,  
 690 M. R., and Young, N.: Geomorphic and geologic controls of geohazards induced by Nepal’s 2015 Gorkha earthquake,  
 691 *SCIENCE*, 351, aac8353, <https://doi.org/10.1126/science.aac8353>, 2016.  
 692 Keefer, D. K.: Landslides caused by earthquakes, *Geol Soc America Bull*, 95, 406, [https://doi.org/10.1130/0016-](https://doi.org/10.1130/0016-7606(1984)95<406:LCBE>2.0.CO;2)  
 693 [7606\(1984\)95<406:LCBE>2.0.CO;2](https://doi.org/10.1130/0016-7606(1984)95<406:LCBE>2.0.CO;2), 1984.  
 694 Kilburn, C. R. J. and Voight, B.: Slow rock fracture as eruption precursor at Soufriere Hills Volcano, Montserrat, *GEOPHYS*  
 695 *RES LETT*, 25, 3665–3668, <https://doi.org/10.1029/98GL01609>, 1998.  
 696 Krautblatter, M., Funk, D., and Günzel, F. K.: Why permafrost rocks become unstable: a rock–ice-mechanical model in time  
 697 and space, *EARTH SURF PROC LAND*, 38, 876–887, <https://doi.org/10.1002/esp.3374>, 2013.  
 698 Lang, K. A., Huntington, K. W., and Montgomery, D. R.: Erosion of the Tsangpo Gorge by megafloods, Eastern Himalaya,  
 699 *GEOLOGY*, 41, 1003–1006, <https://doi.org/10.1130/G34693.1>, 2013.  
 700 Larsen, I. J., Montgomery, D. R., and Korup, O.: Landslide erosion controlled by hillslope material, *NAT GEOSCI*, 3, 247–  
 701 251, <https://doi.org/10.1038/ngeo776>, 2010.  
 702 Li, H., Hu, K., Zhang, X., Liu, S., and Wei, L.: Causes and Damage of the 2020 Periglacial Debris Flows at Zelunglung  
 703 Catchment in the Eastern Syntaxis of Himalaya, in: *Engineering Geology for a Habitable Earth: IAEG XIV Congress 2023*  
 704 *Proceedings, IAEG 2023, Chengdu, China, 21–27 September 2023*, 161–171, [https://doi.org/10.1007/978-981-99-9061-0\\_12](https://doi.org/10.1007/978-981-99-9061-0_12),  
 705 2024.  
 706 Li, J., Chu, H., Li, B., Gao, Y., Wang, M., Zhao, C., and Liu, X.: Analysis of development characteristics of high-  
 707 elevationchain geological hazard in Zelongnong, Nyingchi, Tibet based on high resolution image and InSAR interpretation,  
 708 *The Chinese Journal of Geological Hazard and Control*, 32, 42–50, [https://doi.org/10.16031/j.cnki.issn.1003-8035.2021.03-](https://doi.org/10.16031/j.cnki.issn.1003-8035.2021.03-06)  
 709 [06](https://doi.org/10.16031/j.cnki.issn.1003-8035.2021.03-06), 2021.  
 710 Li, W., Zhao, B., Xu, Q., Scaringi, G., Lu, H., and Huang, R.: More frequent glacier-rock avalanches in Sedongpu gully are  
 711 blocking the Yarlung Zangbo River in eastern Tibet, *LANDSLIDES*, 19, 589–601, [https://doi.org/10.1007/s10346-021-01798-](https://doi.org/10.1007/s10346-021-01798-z)  
 712 [z](https://doi.org/10.1007/s10346-021-01798-z), 2022.



Li Y., Yan C., Hu K., and Wei L.: VARIATION OF HAZARD AREAS OF TYPICAL RAINSTORM DEBRIS FLOW  
 ALLUVIAL FANS, Resources and Environment in the Yangtze Basin, 26, 789–796,  
<https://doi.org/10.11870/cjlyzyyhj201705017>, 2017.

Liu, M., Zhang, Y., Tian, S., Chen, N., Mahfuz, R., and Javed, I.: Effects of loose deposits on debris flow processes in the  
 Aizi Valley, southwest China, J MT SCI-ENGL, 17, 156–172, <https://doi.org/10.1007/s11629-019-5388-9>, 2020.

Liu, W., Lai, Z., Hu, K., Ge, Y., Cui, P., Zhang, X., and Liu, F.: Age and extent of a giant glacial-dammed lake at Yarlung  
 Tsangpo gorge in the Tibetan Plateau, GEOMORPHOLOGY, 246, 370–376, <https://doi.org/10.1016/j.geomorph.2015.06.034>,  
 2015.

Liu, W., Wang, M., Song, B., Yu, T., Huang, X., Jiang, Y., and Sun, Y.: Surveys and chain structure study of potential hazards  
 of ice avalanches based on optical remote sensing technology: A case study of southeast Tibet, Remote Sensing for Natural  
 Resources, 34, 265–276, <https://doi.org/10.6046/zrzyyg.2021076>, 2022.

Liu, Y., Montgomery, D. R., Hallet, B., Tang, W., Zhang, J., and Zhang, X.: QUATERNARY GLACIER BLOCKING  
 EVENTS AT THE ENTRANCE OF YARLUNG ZANGBO GREAT CANYON, SOUTHEAST TIBET, Quaternary Sciences,  
 52–62, <https://doi.org/10.3321/j.issn:1001-7410.2006.01.007>, 2006.

Major, J. J.: Pebble orientation on large, experimental debris-flow deposits, SEDIMENT GEOL, 117, 151–164,  
[https://doi.org/10.1016/S0037-0738\(98\)00014-1](https://doi.org/10.1016/S0037-0738(98)00014-1), 1998.

Martha, T. R., Roy, P., Mazumdar, R., Govindharaj, K. B., and Kumar, K. V.: Spatial characteristics of landslides triggered  
 by the 2015 Mw 7.8 (Gorkha) and Mw 7.3 (Dolakha) earthquakes in Nepal, LANDSLIDES, 14, 697–704,  
<https://doi.org/10.1007/s10346-016-0763-x>, 2017.

McCoy, S. W., Tucker, G. E., Kean, J. W., and Coe, J. A.: Field measurement of basal forces generated by erosive debris flows,  
 J GEOPHYS RES-EARTH, 118, 589–602, <https://doi.org/10.1002/jgrf.20041>, 2013.

Montgomery, D. R., Hallet, B., Yuping, L., Finnegan, N., Anders, A., Gillespie, A., and Greenberg, H. M.: Evidence for  
 Holocene megafloods down the tsangpo River gorge, Southeastern Tibet, QUATERNARY RES, 62, 201–207,  
<https://doi.org/10.1016/j.yqres.2004.06.008>, 2004.

Parker, R. N., Densmore, A. L., Rosser, N. J., de Michele, M., Li, Y., Huang, R., Whadcoat, S., and Petley, D. N.: Mass wasting  
 triggered by the 2008 Wenchuan earthquake is greater than orogenic growth, Nature Geosci, 4, 449–452,  
<https://doi.org/10.1038/ngeo1154>, 2011.

Peng, D., Zhang, L., Jiang, R., Zhang, S., Shen, P., Lu, W., and He, X.: Initiation mechanisms and dynamics of a debris flow  
 originated from debris-ice mixture slope failure in southeast Tibet, China, Engineering Geology, 307, 106783,  
<https://doi.org/10.1016/j.enggeo.2022.106783>, 2022.

Peng, S.: 1-km monthly mean temperature dataset for china (1901-2023), National Tibetan Plateau Data Center [data set],  
<https://doi.org/10.11888/Meteoro.tpd.270961>, 2019.

745 Peng, S.: 1-km monthly precipitation dataset for China (1901-2023), National Tibetan Plateau / Third Pole Environment Data  
 746 Center [data set], <https://doi.org/10.5281/zenodo.3114194>, 2020.

747 Peng, S., Ding, Y., Liu, W., and Li, Z.: 1 km monthly temperature and precipitation dataset for China from 1901 to 2017,  
 748 EARTH SYST SCI DATA, 11, 1931–1946, <https://doi.org/10.5194/essd-11-1931-2019>, 2019.

749 Petrakov, D. A., Krylenko, I. V., Chernomorets, S. S., Tutubalina, O. V., Krylenko, I. N., and Shakhmina, M. S.: Debris flow  
 750 hazard of glacial lakes in the Central Caucasus, in: Debris-Flow Hazards Mitigation: Mechanics, Prediction, and Assessment,  
 751 The Fourth International Conference on Debris-Flow Hazards Mitigation: Mechanics, Prediction, and Assessment, Chengdu,  
 752 China, 10-13 September 2007, 703–714, ISBN 9789059660595, 2007.

753 Richardson, S. D. and Reynolds, J. M.: An overview of glacial hazards in the Himalayas, Quaternary International, 65–66, 31–  
 754 47, [https://doi.org/10.1016/S1040-6182\(99\)00035-X](https://doi.org/10.1016/S1040-6182(99)00035-X), 2000.

755 Shen, Y., Su, H., Wang, G., Mao, W., Wang, S., Han, P., Wang, N., and Li, Z.: The Responses of Glaciers and Snow Cover to  
 756 Climate Change in Xinjiang (II): Hazards Effects, Journal of Glaciology and Geocryology, 35, 1355–1370, 2013.

757 Shugar, D. H., Jacquemart, M., Shean, D., Bhushan, S., Upadhyay, K., Sattar, A., Schwanghart, W., McBride, S., de Vries, M.  
 758 V. W., Mergili, M., Emmer, A., Deschamps-Berger, C., McDonnell, M., Bhambri, R., Allen, S., Berthier, E., Carrivick, J. L.,  
 759 Clague, J. J., Dokukin, M., Dunning, S. A., Frey, H., Gascoin, S., Haritashya, U. K., Huggel, C., Kääb, A., Kargel, J. S.,  
 760 Kavanaugh, J. L., Lacroix, P., Petley, D., Rupper, S., Azam, M. F., Cook, S. J., Dimri, A. P., Eriksson, M., Farinotti, D., Fiddes,  
 761 J., Gnyawali, K. R., Harrison, S., Jha, M., Koppes, M., Kumar, A., Leinss, S., Majeed, U., Mal, S., Muhuri, A., Noetzli, J.,  
 762 Paul, F., Rashid, I., Sain, K., Steiner, J., Ugalde, F., Watson, C. S., and Westoby, M. J.: A massive rock and ice avalanche  
 763 caused the 2021 disaster at Chamoli, Indian Himalaya, Science, 373, 300–306, <https://doi.org/10.1126/science.abh4455>, 2021.

764 Sohn, Y. K.: Coarse-grained debris-flow deposits in the Miocene fan deltas, SE Korea: a scaling analysis, SEDIMENT GEOL.,  
 765 130, 45–64, [https://doi.org/10.1016/S0037-0738\(99\)00099-8](https://doi.org/10.1016/S0037-0738(99)00099-8), 2000.

766 Stoffel, M., Trappmann, D. G., Coullie, M. I., Ballesteros Cánovas, J. A., and Corona, C.: Rockfall from an increasingly  
 767 unstable mountain slope driven by climate warming, NAT GEOSCI, 17, 249–254, [https://doi.org/10.1038/s41561-024-01390-](https://doi.org/10.1038/s41561-024-01390-9)  
 768 9, 2024.

769 Tian, L., Yao, T., Gao, Y., Thompson, L., Mosley-Thompson, E., Muhammad, S., Zong, J., Wang, C., Jin, S., and Li, Z.: Two  
 770 glaciers collapse in western Tibet, J GLACIOL, 63, 194–197, <https://doi.org/10.1017/jog.2016.122>, 2017.

771 Wang, J., Jin, Z., Hilton, R. G., Zhang, F., Densmore, A. L., Li, G., and West, A. J.: Controls on fluvial evacuation of sediment  
 772 from earthquake-triggered landslides, Geology, 43, 115–118, <https://doi.org/10.1130/G36157.1>, 2015.

773 Wang, P., Wang, H., Hu, G., Qin, J., and Li, C.: A preliminary study on the development of dammed paleolakes in the Yarlung  
 774 Tsangpo River basin, southeastern Tibet, Earth Science Frontiers, 28, 35–45, <https://doi.org/10.13745/j.esf.sf.2020.9.18>, 2021.

775 Wang, Z., Hu, K., and Liu, S.: Classification and sediment estimation for debris flow-prone catchments in the Parlung Zangbo  
 776 Basin on the southeastern Tibet, Geomorphology, 413, 108348, <https://doi.org/10.1016/j.geomorph.2022.108348>, 2022.

Wang, Z., Ma, C., Hu, K., Liu, S., and Lyu, L.: Investigation of initiation conditions of periglacial debris flows in Sanggu watershed, Eastern Himalayas, Tibet Plateau (China), *LANDSLIDES*, 20, 813–827, <https://doi.org/10.1007/s10346-022-02003-5>, 2023.

Ward, F. K.: Explorations in South-Eastern Tibet, *GEOGR J*, 67, 97, <https://doi.org/10.2307/1783136>, 1926.

Yan, Y., Tang, H., Hu, K., Turowski, J. M., and Wei, F.: Deriving Debris-Flow Dynamics From Real-Time Impact-Force Measurements, *J GEOPHYS RES-EARTH*, 128, e2022JF006715, <https://doi.org/10.1029/2022JF006715>, 2023.

Yang, A., Wang, H., Liu, W., Hu, K., Liu, D., Wu, C., and Hu, X.: Two megafloods in the middle reach of Yarlung Tsangpo River since Last-glacial period: Evidence from giant bars, *GLOBAL PLANET CHANGE*, 208, 103726, <https://doi.org/10.1016/j.gloplacha.2021.103726>, 2022.

Yu, G.-A., Yao, W., Huang, H. Q., and Liu, Z.: Debris flows originating in the mountain cryosphere under a changing climate: A review, *Progress in Physical Geography: Earth and Environment*, 45, 339–374, <https://doi.org/10.1177/0309133320961705>, 2021.

Zhang, G., Yao, T., Xie, H., Yang, K., Zhu, L., Shum, C. K., Bolch, T., Yi, S., Allen, S., Jiang, L., Chen, W., and Ke, C.: Response of Tibetan Plateau lakes to climate change: Trends, patterns, and mechanisms, *EARTH-SCI REV*, 208, 103269, <https://doi.org/10.1016/j.earscirev.2020.103269>, 2020.

Zhang, J. and Shen, X.: Debris-flow of Zelongnong Ravine in Tibet, *J. Mt. Sci.*, 8, 535–543, <https://doi.org/10.1007/s11629-011-2137-0>, 2011.

Zhang, T., Li, D., East, A. E., Walling, D. E., Lane, S., Overeem, I., Beylich, A. A., Koppes, M., and Lu, X.: Warming-driven erosion and sediment transport in cold regions, *NAT REV EARTH ENV*, 3, 832–851, <https://doi.org/10.1038/s43017-022-00362-0>, 2022a.

Zhang W.: Some features of the surge glacier in the MT. Namjagbarwa, *Mountain Research*, 234–238, 1985.

Zhang, W.: Identification of glaciers with surge characteristics on the Tibetan Plateau, *Ann. Glaciol.*, 16, 168–172, <https://doi.org/10.3189/1992AoG16-1-168-172>, 1992.

Zhang, X., Hu, K., Liu, S., Nie, Y., and Han, Y.: Comprehensive interpretation of the Sedongpu glacier-related mass flows in the eastern Himalayan syntaxis, *J. Mt. Sci.*, 19, 2469–2486, <https://doi.org/10.1007/s11629-022-7376-8>, 2022b.

Zhou, G. G. D., Li, S., Song, D., Choi, C. E., and Chen, X.: Depositional mechanisms and morphology of debris flow: physical modelling, *LANDSLIDES*, 16, 315–332, <https://doi.org/10.1007/s10346-018-1095-9>, 2019.

Zhu, S., Wu, W., Zhao, X., Li, J., and Wang, H.: Middle-Late Pleistocene Glacial Lakes in the Grand Canyon of the Tsangpo River, Tibet, *Acta Geologica Sinica (Eng)*, 86, 266–283, <https://doi.org/10.1111/j.1755-6724.2012.00627.x>, 2012.